DROPLET DECARBURIZATION KINETICS IN STEELMAKING SLAGS

DECARBURIZATION KINETICS OF FE-C-S DROPLETS IN OXYGEN STEELMAKING SLAGS

By

MICHAEL POMEROY, B.ENG.

A Thesis

Submitted to the School of Graduate Studies

in Partial Fulfillment of the Requirements

for the Degree

Master of Science

McMaster University

MASTER OF SCIENCE (2011) McMaster University

(Materials Science) Hamilton, Ontario

TITLE: Decarburization Kinetics of Fe-C-S Droplets in Oxygen Steelmaking Slags

AUTHOR: Michael Pomeroy, B.Eng. (McMaster University)

SUPERVISOR: Professor Kenneth S. Coley

NUMBER OF PAGES: x, 72

Abstract

The slag metal emulsion may play a significant role in the global furnace decarburization kinetics in oxygen steelmaking. In recent years, the important interaction between droplet generation rate, droplet residence time in slag and droplet decarburization rate has become more evident in the literature. The decarburization kinetics of Fe-C-S droplets in CaO-SiO2-MgO-FeO slags were investigated for higher carbon droplets (approximately 4.2 % C). The effect of slag FeO, droplet mass and Sulphur content on decarburization rate were evaluated. The limit between external and internal nucleation of CO gas was investigated. A model was developed for prediction of time to the onset of carbon boil.

Acknowledgements

I would like to extend my deep and sincere gratitude to my supervisor, Dr. Ken Coley, for his support and guidance over all my years at McMaster University. I am hard pressed to recall leaving a meeting with Dr. Coley feeling unmotivated. His support has always left me enthusiastic about the task at hand. My supervisor's seemingly boundless passion for our research and process metallurgy in general has been a great inspiration to me both academically and professionally.

I would also like to extend a great many thanks to my graduate student colleagues in Dr. Coley's research group. In particular I would like to thank Elaine Chen for much patience in training me on the research apparati over the years, and Glendon Brown for countless hours of support as we worked through the various experimental issues that inevitably arise.

I would like to thank the Materials Science and Engineering department at McMaster University, both faculty and staff, for many useful conversations and debates. I am deeply indebted to the broader population of graduate students in the department, along with the departmental staff, particularly Diana Maltese, Nanci Cole and Owen Kelly. I would like to thank the McMaster Steel Research Centre for providing the framework for the research along with NSERC for funding this project.

Finally I would like to extend my sincere thanks to my family for the encouragement and support in pursuing all things academic. Without their patience and understanding of my many absences I would have been unable to complete this thesis.

Table of Contents

List of Figures and Illustrations

Abbreviations and Symbols

Symbols

A_i	Interfacial area at location *i* in cm^2
a_i	Activity of component i relative to pure substance *i*
C_i	Concentration of an element in mol / cm^3
F_i	Force component i in N
f_i	Henrian 1 % standard activity coefficient of component *i*
H	Enthalpy (J / mol)
h_i	Activity of component *i* relative to Henrian 1 % standard
J_i	Flux of element *i* in mol / cm^2 s
K_i	Equilibrium coefficient for reaction *i*
k_i	Kinetic rate constant in g / cm^2 s or mol / cm^2 s
M_i	Molecular weight of substance *i* (g / mol)
m_i	Mass transfer coefficient of a species in medium *i* in cm / s
MW_i	Molecular weight of species *i* (g/mol)
N_B	Dimensionless Blowing number
N_O	Number concentration of embryos in droplet (embryos / m^3)
p_i	Partial Pressure of a gaseous species *i* in atm
R	Gas constant
T	Absolute Temperature (K)
α	Constant relating measured pressure change to moles gas (mol / PSI)
γ	Activity coefficient of component i in slag
δ	Distance from interface (m)
θ_i	Fraction of surface sites occupied by component i
μ_i	Chemical potential of species i
ρ_i	Density of species i in g / cm^3
σ	Interfacial Surface Tension (N / m)
Ψ	Surface tension modifying parameter

Accents

[*i*]	Concentration of I in metal (weight %)
(*i*)	Concentration of I in slag (weight %
$\rightarrow$	Forward Reaction
$\leftarrow$	Backward Reaction
$\underline{i}$	Species *i* dissolved in iron

Subscripts

ads	adsorbed
eq	equilibrium
g	gas
l	liquid
s	slag
v,e	equilibrium vapour

Declaration of Academic Achievement

The present study seeks to expand the body of knowledge regarding the existence of two separate kinetic regimes in the droplet decarburization reactions in oxygen steelmaking slags. Experiments carried out by the author generated kinetic data over a range of steelmaking conditions. Analysis of the experimental results, and the development of a numerical model, help advance the understanding of the onset of internal gas evolution in droplets. The present work should help advance the understanding of the global decarburization kinetics in modern oxygen steelmaking converters.

Chapter I

Introduction

1.1 Motivation for This Study

The use of oxygen for the decarburization of hot iron is no recent addition to the global steel industry. Experiments in the use of roof lances in the United States in the first half of the last century eventually led to the development of the LD furnace, also known as the Basic Oxygen Furnace or BOF[1]. Originally introduced as a novelty 35 tonne furnace in Linz, Austria, the BOF is now responsible for the overwhelming majority of the refining of hot iron into steel worldwide[1].

The acceptance of the process can be attributed to many factors. A few have been suggested[1] such as the ability to melt a large amount of scrap with each heat, generally rapid decarburization (compared to earlier processes), lower quantities of smoke and fume and lower final oxygen, nitrogen, hydrogen, sulphur and oxygen contents.

Research began in earnest in the 1960s to gain a more mature understanding of the global decarburization kinetics within the furnace. Meyer *et al.* may have been the first to conduct a significant mechanistic study[2] of refining rates in BOFs. These authors suggest in their study that a so-called slag-metal emulsion is principally responsible for the rapid observed decarburization rates. This "emulsion" is the result of surface instabilities created by the high velocity oxygen jet on the surface of the melt throwing droplets into the furnace slag.

This slag-metal emulsion plays a potentially significant role in BOF decarburization. These workers also proposed the existence of an external gas halo reaction regime, followed by the onset of internal nucleation of bubbles, concepts upon which subsequent work has built.

Early qualitative evidence for the importance of the emulsion in overall kinetics was drawn from the large amount of iron observed in the slag (up to 50% of furnace metal being found in the slag-metal "emulsion"[2]), coupled with the lower carbon content of droplets compared to the simultaneous bath carbon content

Numerous studies[2-16] have been carried out over the years regarding the enhanced kinetics of droplet decarburization. Recent work by Subagyo[17] showed that a simple Stokes' Law force balance upon a droplet generated with a given kinetic energy predicts residence times that are up to 60 times lower than required to support the refining rates observed in practice.

This discrepancy was later reconciled by Brooks et al.[18], who showed that residence times consistent with observed refining rates could be obtained if one considered the swelling of droplets due to internal nucleation of gas.

In an attempt to establish an overall mechanism for this process,, an extensive study[19,20] of the kinetics of the internal decarburization reaction was undertaken by Chen. It was observed, as in the case Molloseau[13], that at higher slag oxygen potentials the droplets swell due to the internal nucleation of CO gas, so called "carbon boil".

The slag-metal emulsion quite possibly plays a significant role in the global decarburization kinetics of the furnace. Up to 50 % of furnace metal may be found entrained in the slag during the blow[2]. Slag borne droplets have been found to exhibit carbon contents between 33 and 70 percent lower than the simultaneous bath carbon content[3]. Some researchers have suggested that approximately 35% of total decarburization is carried out in the slag-metal emulsion[21]. Since the carbon boil can increase the observed decarburization rate up to 6 fold over the external decarburization regime[13,19-20] and increase the droplet residence time in slag over 60 fold[18], understanding its onset may be of fundamental importance to global furnace refining rates.

1.2 Objectives of This Study

Chen[19,20] has already developed a predictive kinetic model for droplet swelling rates over a range of BOF conditions. The objective of this study is to gain an understanding of the transition from the external "halo" decarburization reaction regime to the internal nucleation of CO bubbles or "carbon boil" kinetic regime. The specific objectives of this study are outlined as follows:

1. To obtain reliable experimental kinetic data over a range of oxygen steelmaking conditions (slag composition, metal chemistry and droplet size).

2. To gain a more detailed understanding of the conditions for the onset of carbon boil.

3. To develop a model capable of predicting the onset of transition from external to internal decarburization.

1.3 Organization of this Thesis

This thesis consists of a literature review, description of experimental methods, presentation of experimental results and theoretical analysis of results including development of the predictive model. Chapter 1 presents the background and motivation for the study. Chapter 2 presents the literature review of past studies. Chapter 3 presents the experimental program and apparatus. Chapter 4 gives the results and analysis, including numerical model development.

Chapter II

Literature Review

2.1 Early Works on Slag Metal "Emulsions"

The slag-metal emulsion decarburization proposed by Meyer *et al.* based on their observations involves the following steps[2]:

1) Ejection of metal droplets into the slag phase
2) Transfer of oxygen into metal droplets by unsteady state diffusion. It is proposed that because the droplets exist for some time without any CO gas evolution, a significant supersaturation (of oxygen) is obtained relative to the reaction (where $\underline{C}$ is dissolved Carbon and $\underline{O}$ is dissolved oxygen).

$$\underline{C} + \underline{O} \rightarrow CO \qquad (2.1)$$

3) Metal droplets saturated in oxygen contact bubbles of CO ascending through the slag. At this point, it is proposed that CO evolution occurs violently at the droplet surface (no ascending CO gas in the slag present in the current study).
4) Metal droplets become supersaturated with oxygen to such an extent that internal nucleation of CO begins.

Removal of carbon from the droplets attributed to carbon diffusion to the surface was ruled out[2] as the rate determining step and not considered since in this case, refining rates would decrease with continuing decarburization, which was not observed in the

experiments. No rate determining step was suggested. The possibility that steps 2, 3 and 4 occur simultaneously was noted.

The study[2] of Meyer *et al.* was relevant because it brought to light the potentially significant role played by the slag-metal emulsion in BOF decarburization. It also proposed the existence of an external gas halo (surface decarburization), followed by the onset of internal nucleation of droplets (carbon boil), concepts upon which subsequent work has built.

Kozakevitch[4] also noted the potential existence of two gas regimes for the CO bubbles: what he described as a "lens-shaped cavity" at the surface (Figure 2.1), and a "blow hole" with internal nucleation. Kozakevitch[4] attributed these to a surface adhesion of bubbles to surface of the droplet. The observation leading to his conclusion can be seen in Figure 2.1:

Figure 2.1: "Lens shaped cavities" observed by Kozakevitch. Source: [4]

2.2 Kinetic Studies of Droplet Decarburization in FeO Bearing Slags

Mulholland, Hazeldean and Davies undertook an extensive study[5] by X-Ray fluoroscopy of the droplet decarburization reactions in question. The effect of droplet size, slag composition, temperature, metal composition and oxygen blowing were considered. Gas evolution was not studied, so the only observed effect of drop size was the higher buoyancy of smaller droplets. It was observed that smaller droplets were always attached to gas bubbles, perhaps lending support to Kozakevitch's[4] initial suggestion. Slag composition was observed to have a significant impact on the reaction, with more oxidizing slags (higher Fe_2O_3) resulting in a more violent decarburization. In their study, temperature was observed to be unimportant in determining the decarburization rate. This may in part be due to the lack of CO evolution measurement, which in other studies[8,18] appeared to be influenced by the temperature according an Arrhenius relationship.

CO nucleation was observed both at the slag/metal interface and internally. The following mechanism was proposed[5] in the presence of a gas halo surrounding the droplet, where O_{ads} represents adsorbed oxygen at the surface:

1) Oxygen mass transport in slag
2) Charge transfer: Either

$$2Fe^{3+} + O^{2-} = 2Fe^{2+} + O_{ads} \quad (2.2)$$

or

$$Fe^{2+} + O^{2-} = Fe \quad + O_{ads} \quad (2.2)$$

3) The reaction

$$CO + O_{ads} = CO_2 \tag{2.3}$$

at the halo/slag interface and

$$CO_2 + \underline{C} = 2CO \tag{2.4}$$

at the gas/metal interface

4) Interface adsorption or desorption of CO and CO2.

It is also suggested by Mulholland[5] that the following reactions also take place in the foam:

$$CO + 2Fe^{3+} + O^{2-} = 2Fe^{2+} + CO_2 \tag{2.5}$$

and

$$CO + Fe^{2+} + O^{2-} = Fe + CO_2. \tag{2.6}$$

A schematic diagram of a gas halo reduction regime is presented in Figure 2.2:

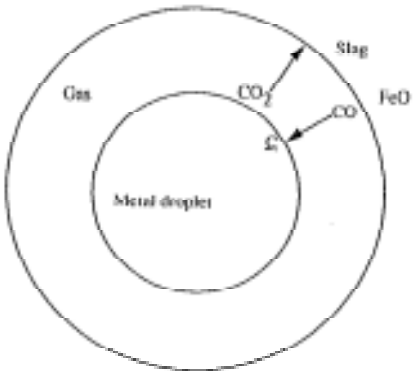

Figure 2.2: Schematic of the halo regime. Source: [7]

Mulholland[5] intentionally avoided interpreting one step to be slower or controlling due to the lack of activity at the time in the field. However they did point out that since the reaction was much more rapid in the foam than in the slag, the nucleation of bubbles or gas phase transport may be important. It is also noted that in the presence of a gas halo, the reaction goes only as fast as CO_2 can be produced and transported.

Min and Fruehan[6] studied the rate of decarburization in the halo regime using X-ray fluoroscopy and measurement of gas evolution flow rates. The primary reactions considered were the gas/slag interface reaction

$$CO + (FeO) = Fe + CO_2 \quad (2.7)$$

where (FeO) represents slag dissolved FeO, followed by the gas-metal reaction

$$CO_2 + \underline{C} = 2CO \quad (2.8)$$

Five possible rate determining steps were considered[6]:

1) FeO (Fe^{2+} and O^{2-}) transport to the gas-slag interface in the slag.
2) Rate of the slag-gas reaction, equation (2.7)
3) Diffusion of gaseous species in the halo
4) Carbon mass transfer in the droplet
5) Rate of the metal-gas reaction, equation (2.8)

The rate was found to be a function of droplet size, FeO content, C content and S content. The gas slag reaction was broken down into several steps[6]:

1) $CO\ (g) = CO\ (surface)$
2) $(FeO) = Fe^{2+} + O^{2-}$
3) $CO_{ads} + O^{2-} = CO_2 + 2e^-$
4) $Fe^{2+} + 2e^- = Fe$

An overall rate, R_{g-s}, for the gas slag reaction is given[6] as

$$R_{g-s} = k_{g-s}(p_{co}a_{FeO} - p_{CO}^{eq}a_{FeO}^{eq}) \quad (2.9)$$

where k_{g-s} is the forward rate constant for the gas-sold reaction, p_{co} is the partial pressure of CO at the gas-slag interface, a_{FeO} is the activity of FeO at the gas-slag interface, p_{CO}^{eq} is the equilibrium CO partial pressure at the interface and $a_{FeO}^{eq}$is the activity of FeO at its equilibrium value at the interface. The flux of FeO, J_{FeO}, was calculated by

$$J_{FeO} = m_s(C_{FeO} - C_{FeO}^{bulk}) \quad (2.10)$$

where m_s is the mass transfer coefficient for FeO in the slag, C_{FeO} is the concentration of FeO at the interface, and C_{FeO}^{bulk} is the bulk slag FeO concentration. Gas diffusion, the transfer of CO_2 in the halo, was calculated according to[6]

$$(CO_2)_{g-s} \rightarrow (CO_2)_{g-m} \quad (2.11)$$

$$J_{CO2} = \frac{m_g}{RT} \ln \frac{1+p_{CO2}^{s}}{1+p_{CO2}^{m}} \quad (2.12)$$

where J_{CO2} is the flux of CO_2 within the halo, m_g is the mass transfer coefficient of CO_2 in the gas, R is the gas constant, p^s_{CO2} is the partial pressure of CO2 at the slag-gas interface, p^m_{CO2} is the CO2 partial pressure at the metal-gas interface and T is the absolute temperature, with the overall rate of reaction, R_g, being given by

$$R_g = \frac{A_s + A_m}{2} \frac{m_g K C}{RT} (\%FeO) \tag{2.13}$$

where A_s and A_m are interfacial areas of the slag-gas interface and gas-metal interface respectively, K is the equilibrium constant for the slag-gas interface reaction, equation (2.7), and C is the constant relating activity to weight percent for FeO.

The gas metal reaction rate, R_{g-m}, was assumed to vary according to[6]:

$$R_{g-m} = k_{CO2} A_m \left(p^m_{CO2} - p^{eq}_{CO2}\right) \tag{2.14}$$

where k_{CO2} is the forward rate constant for the gas-metal reaction, equation (2.8), p_{CO2} is the partial pressure of CO_2 at the gas-metal interface and p^{eq}_{CO2} is the partial pressure of CO_2 in equilibrium with reaction (2.8). Reaction (2.14) was also presented in terms of FeO content,

$$R_{g-m} = k_{CO2} A_m K \quad C(\text{pct FeO}) \tag{2.15}$$

with K now the equilibrium constant for the gas-metal reaction (2.8), C relating activity to weight percent for FeO, and k_{CO2} being the rate constant for reaction (2.8), a function of sulphur content.

Some data from other workers[10] was used in the comparison of rate constants in [6]. The obtained overall rate constants were somewhere between those obtained for certain steps[6]. Consequently a mixed control rate model was proposed with steps 1, 3 and 5 controlling. Therefore the rate was given by

$$\text{Rate} = k_0(\%\text{FeO}) \tag{2.16}$$

with the constant given by

$$k_0 = \frac{1}{\frac{2RT}{K_{sg}C(A_s+A_m)}+\frac{100(MW)_{FeO}}{m_s\rho A_s}+\frac{1}{k_{CO2}A_m K_{mg}C}} \tag{2.17}$$

where k_0 is the mixed control rate constant, MW_{FeO} is the molar mass of FeO and ρ is the slag density.

It was suggested[6] that at low sulphur contents (fast overall metal-gas reaction) that the dependence on the metal gas reaction is eliminated and only slag phase transport and gas transport in the halo are significant in determining rate. For higher sulphur contents it was suggested[6] that the gas metal reaction becomes rate controlling.

Murthy *et al.*[8],[9] studied FeO reduction in oxidizing slags by Fe-C droplets, again considering the existence of a gas halo. Considering the effect of FeO, the overall reaction was suggested to follow 1st order kinetics with respect to FeO and 0th order with respect to C:

$$\text{Rate} = kC_{FeO}^{slag} \tag{2.18}$$

where k is the overall rate constant. The variation of rate with FeO content obtained in Murthy's study is shown in Figure 2.3:

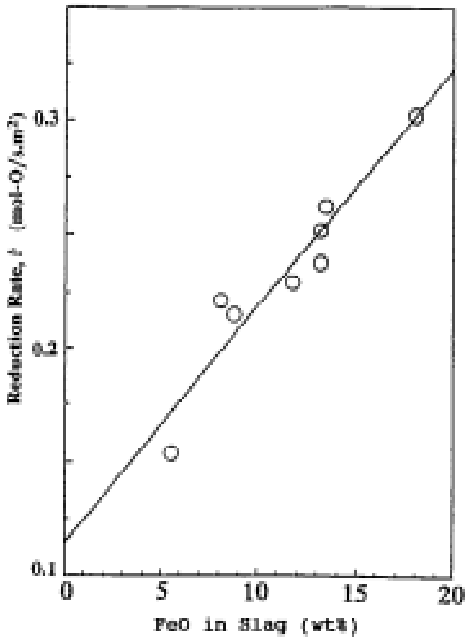

Figure 2.3: Variation of rate with FeO by Murthy. Source: [8]

Temperature was found to follow an Arrhenius relationship as shown in Figure 2.4.

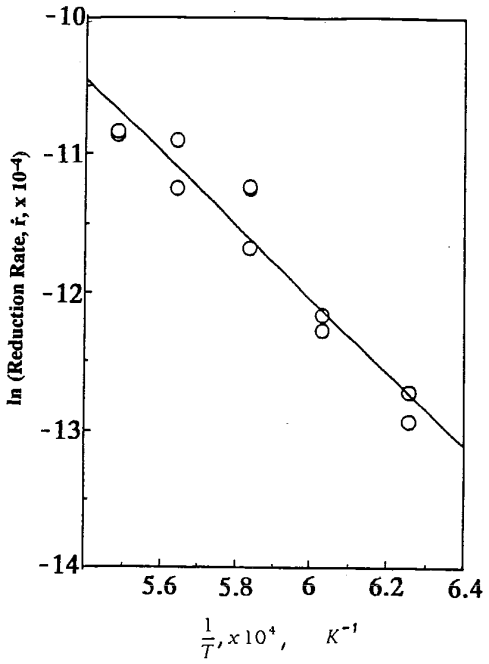

Figure 2.4: Variation of rate with temperature. Source: [8]

The potential rate limiting steps considered[9] were similar to those in other studies:

1) Carbon transport from droplet bulk to gas metal interface
2) Gas metal interface chemical reactions
3) Gas transport in the gas halo
4) Gas slag chemical reactions
5) FeO transport in slag directly adjacent to the gas halo
6) Bulk slag FeO transport

Carbon transport in the bulk metal was ruled out as rate limiting by dropping droplets of different sizes into the slag: In one case, only one large droplet was dropped and in the second case 5 smaller droplets with total mass equal to the larger droplet were

dropped[9]. The initial rates of reaction for both cases were found to be about the same, ruling out the mass transport of carbon as a rate determining step. A distinct change in mechanism is noted when [C] dropped below 3.8% C[9]. Although the authors do not elaborate, it is likely that this represents the transition to the internal nucleation regime.

A complicated model is developed by Murthy *et al*.[9] to explore the possibility of gas halo transport control. Indeed it was shown feasible[9] that transport in the halo controls the reaction, but it is proposed that because of the frequent collapses of the halos the gas phase transport cannot be the only rate controlling mechanism.

The transport of FeO is considered in two steps: transport in slag directly adjacent to the halo and bulk transport (diffusion from large distances from the interface)[9]. Transport adjacent to the gas halo, in what the authors[9] called the boundary layer, is considered as a transport of ferrous, ferric and oxygen ions and electrons with the condition of the electroneutrality of the layer.

A schematic for this boundary layer is presented in Figure 2.5:

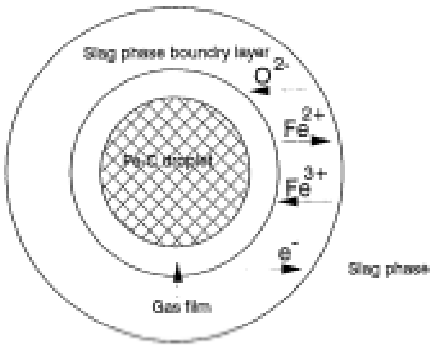

Figure 2.5: Boundary laryer slag diagram. Source: [9]

The authors note[9] that the initial and final rates of reduction would increase if the electronic conductivity of the slag, or electronic transference number t_e were increased. Slag phase mass transport and gas film diffusion were suggested to be the rate determining steps in decarburization with the presence of the halo[9].

Gare and Hazeldean[11] conducted a similar study in which they observed the presence of a gas halo. Like Meyer *et al.*, Gare and Hazeldean consider not rate controlling steps but outline the observed stages of the reactions. These are:

1) Induction period: Low gas evolution
2) Fast external decarburization: Rate increase, existence of a halo
3) Lull Period: Halo begins to subside, slag foam collapses
4) External-Internal nucleation period: Rate begins to increase, with increasing amounts of gas being produced inside the droplet
5) Internal nucleation period: droplet pulsates due to internal gas formation.

The internal nucleation reaction, equation (2.1), is assumed to proceed once the solubility product [C][O] in the metal attained a threshold value[11].

The various decarburization periods described[11] are presented in Figure 2.6:

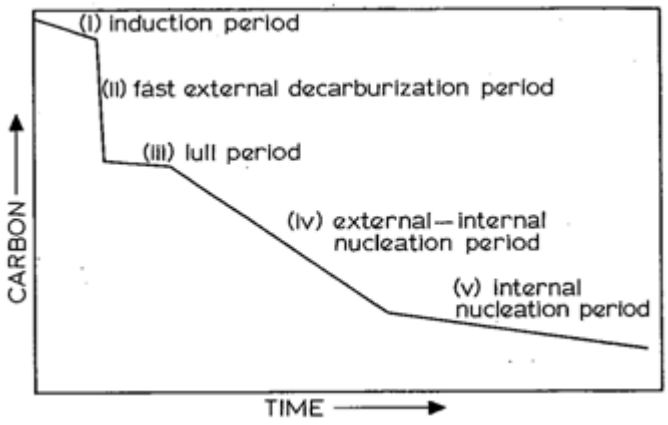

Figure 2.6: Course of decarburization considered by Gare and Hazeldean. Source: [11]

During the induction period, enough oxygen must diffuse into the droplet to begin decarburization[11]. The increasing oxygen content increases the [C][O] product to the point that nucleation of CO can begin[11].

The fast external decarburization period is suggested to be characterized by the presence of the gas halo and a rapid reaction[11]. The gas slag reactions taking place at this point are[11]

$$CO + 2(Fe^{3+}) + (O^{2-}) = 2(Fe^{2+}) + CO_2 \quad (2.19)$$

and

$$CO + 2(Fe^{2+}) + (O^{2-}) = 2(Fe\ ) + CO_2 \quad (2.20)$$

where rounded bracket quantities represent species dissolved in slag. The gas metal reaction is reaction (2.8). It is suggested that the halo stage persists until the gas halo

becomes so wide that gaseous diffusion becomes rate limiting[11], as observed by other workers[6],[8],[9]. The external decarburization period ends while the surface carbon cannot be replaced by bulk carbon from the droplet[11]. The onset of the so-called lull period represents the destabilization and collapse of the gas halo[11]. During the internal-external nucleation period, it is hypothesized that carbon gradients exist inside and at the surface of the droplet, causing a mixed nucleation and bubbling regime[11]. Once surface carbon has been exhausted and carbon is sufficiently low, it is suggested that the internal regime begins[11].

Gaye and Riboud[12] observed similar behaviour to that noted in [11]. More emphasis was placed on the swelling of the droplets at lower carbon levels[12]. The behaviour is described as "emulsification" of the droplet[12]. Although they did not employ X-Ray visualization techniques in their experimental method, an increase in interfacial area of the droplet was noted. Variation of the "emulsification" with droplet sulphur content was also studied at various sulphur contents[12].

Molloseau and Fruehan[13] conducted a thorough study of similar reaction behaviour with more emphasis on quantitative rate measurement than the previous studies. Five steps were considered to be possibly rate determining[13]:

1) The metal gas reaction, equation (2.8).
2) The slag gas reaction, equation (2.7)
3) FeO transfer in the slag
4) Diffusion of C in the metal

5) Diffusion of the CO-CO_2 mixture through the halo.

The most significant results in this case were those obtained at higher FeO levels, where a distinct transition in initial decarburization behaviour is evident[13]. Figure 2.7 shows the effect of FeO content on rate (although the rate was not normalized to an area):

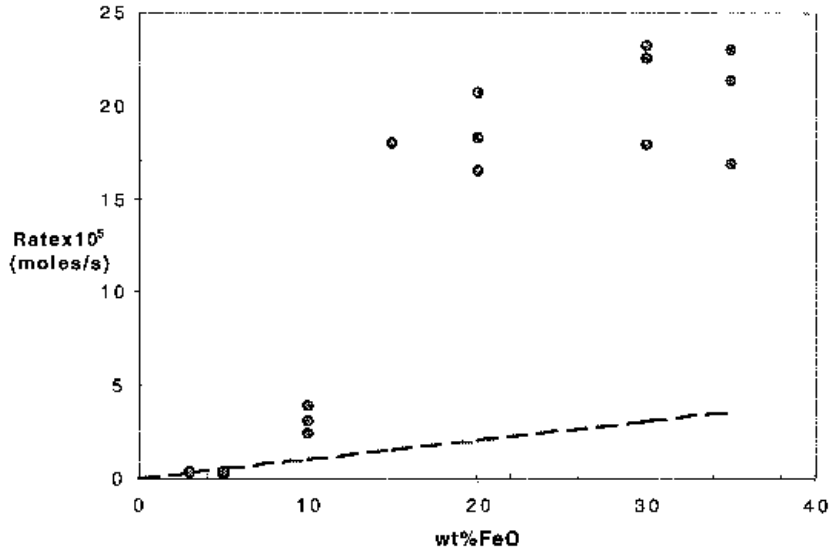

Figure 2.7: Change in decarburization regime with FeO content. Source: [13]

The dashed line in Figure 12 represents the expected behaviour if the reaction were controlled by the metal gas reaction at the droplet surface, which evidently holds only for low FeO contents[13]. Hence it is clear the decarburization rate accelerates significantly in the presence of higher FeO contents. This is in striking contrast to the observations of Murthy, who fit the behaviour with a straight line for these FeO contents[8].

Sun[14] conducted numerical calculations based on an array of previously reported kinetic data. Silicon oxidation at the interface was also considered[14]. Both external and

external nucleation of CO bubbles were incorporated into the calculations[14] as shown in Figure 2.8:

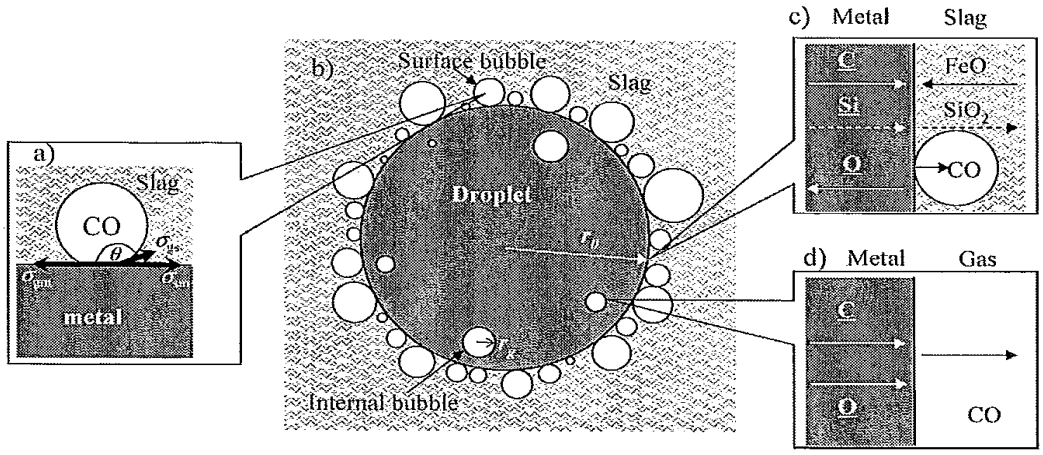

Figure 2.8: Bubbles considered by Sun. Source: [14]

The possible rate controlling steps considered are shown schematically in Figure 2.9, with those steps with an asterisk having been previously determined to be fast[14]:

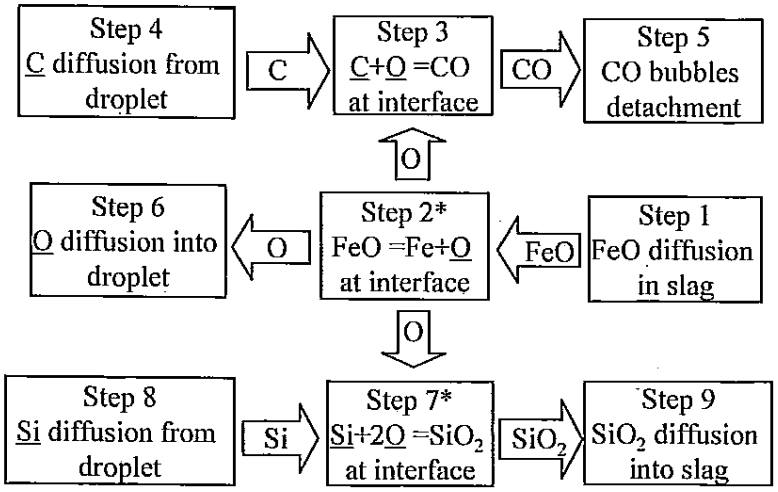

Figure 2.9: Steps considered by Sun. Source: [14]

Droplet swelling, or so called "boiling" has been observed in the past by Baker *et al.*[15]. In the experiments, the droplet was observed to explode while falling through oxygen gas[15]. The implication of this qualitative observation is that at high enough oxygen potentials, nucleation of CO can indeed occur at the inside of a droplet. This is consistent with the observations of several of the studies considered[18,12]. An image of an exploding droplet with internal nucleation can be seen in Figure 2.10:

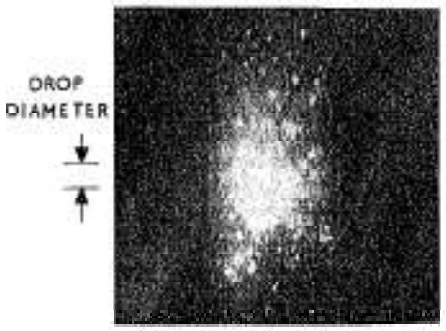

Figure 2.10: Exploding Fe-C droplet in oxygen atmosphere. Source: [15]

It is clear that in a more oxidizing atmosphere, as seen shown in [16], more internal nucleation can occur. This is in accord with other workers[5, 13] who noted that increasing supply of oxygen leads to more violent reaction and increased internal nucleation.

2.3 Interplay between Droplet Generation, Residence and Decarburization

Work conducted at McMaster on droplet residence times applied a Stoke's law expression to falling droplets[17]. Under Stoke's motion, the typical force balance for a droplet can be seen in Figure 2.11:

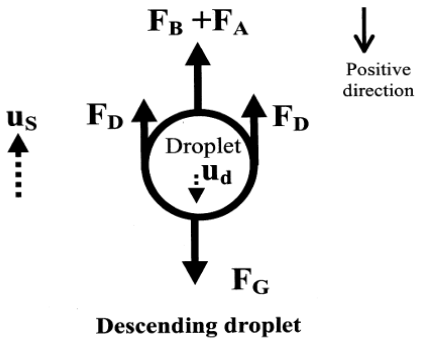

Figure 2.11: Force balance for Stokes motion of a droplet. Source: [17]

where the forces are gravity, buoyancy, drag and "added mass", whereby the droplet accelerates adjacent liquid with it[17].

Droplet generation was found to follow a dimensionless number developed based on the Kelvin-Helmholtz criterion of interfacial stability, the blowing number, N_B, [17],

$$N_B = \frac{\rho_g u_g^2}{2\sqrt{\rho_l g \sigma}} \tag{2.21}$$

where ρ is density of the gas, g is the gravitational constant, σ is the surface tension and u_g is the gas velocity. Larger droplets were found to be ejected from the droplet surface with lower velocity (Figure 2.15).

Brooks *et al*[18] used data from the study on generation of Subagyo[17] to calculate residence times for droplets of various masses and ejection angles. Residence times of less than 1 second were predicted in the absence of chemical reaction, compared with residence times in excess of 1 minute predicted based on refining rates. Brooks *et al*[18]

showed that this discrepancy can be accounted for by considering droplet swelling, the internal evolution of CO gas lowering the overall density.

To obtain more extensive kinetic data on the droplet swelling and internal reaction kinetics, Chen[19,20] undertook an extensive study. To mechanistically describe the swelling regime, the following steps are suggested by Chen[19]:

1) Slag phase mass transfer of O
2) The reaction $Fe^{2+} + O^{2-} = Fe + O_{ads}$ (charge transfer).
3) Diffusion of O into the droplet
4) Diffusion of C in the droplet to the surface
5) CO bubble nucleation
6) Escape of CO from the metal

Significantly, and in contradiction to the conclusions of Gaye and Riboud[12], and Molloseau and Fruehan[13], it was observed that the droplet does not explode and emulsify into tiny droplets. Instead, the droplets were observed to expand due to significant gas evolution[18].

As with Molloseau[13], the rate (of CO evolution) was found to be a strong function of slag FeO content[19]. This can be seen in Figure 2.12:

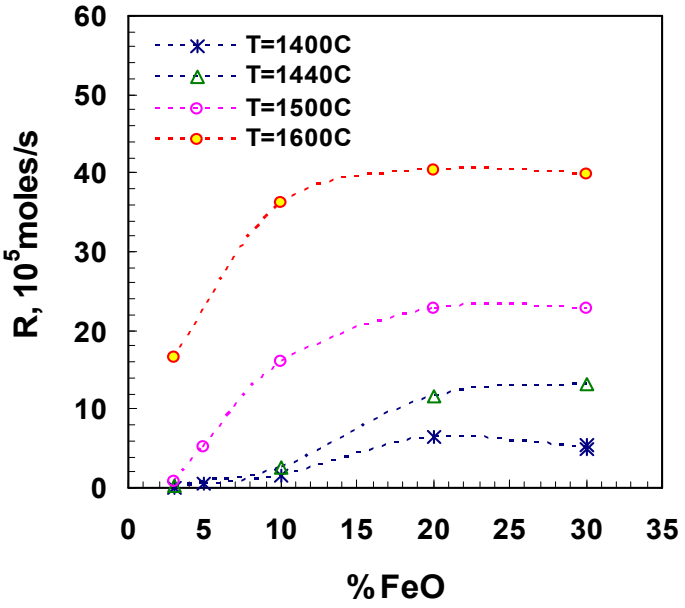

Figure 2.12: Variation of CO evolution rate with FeO content obtained by Chen. Source: [20]

Temperature was observed to follow an Arrhenius relation[19] as is evident in Figure 2.13:

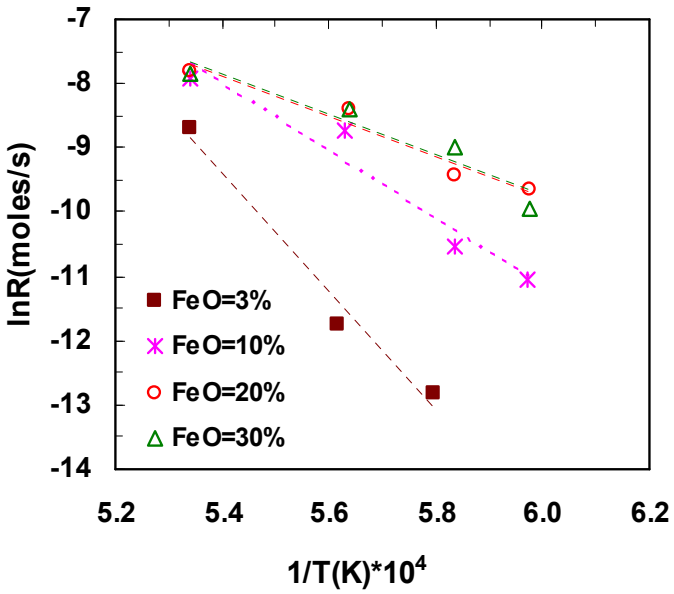

Figure 2.13: Variation of CO evolution with temperature reported by Chen. Source: [20]

Rate was found to increase linearly with droplet mass[18], as shown in Figure 2.14:

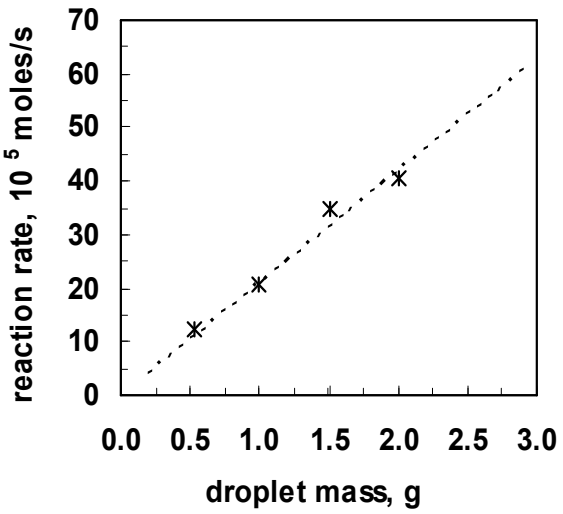

Figure 2.14: Variation of rate with droplet mass according to Chen. Source: [20]

The variation of evolution rate with sulphur content is shown in Figure 2.15:

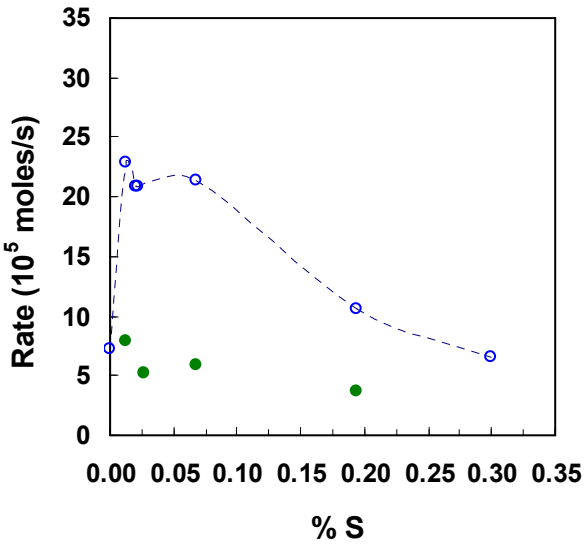

Figure 15: Variation of reaction rate with S content. Source: [20]

As previously mentioned, in the Chen and Coley study[19] the maximum in rate as a function of % S was observed to occur at 0.012 wt %. The explanation for the observed behaviour is that the sulphur lowers the surface tension of the interface, facilitating the reaction, but in increasing amounts poisons the reaction surface by occupying potential reaction sites[19].

A summary of the previous kinetic studies of the slag-metal system under consideration is presented in Table 2.1.

Table 2.1 : Summary of Steps Considered in Decarburization Mechanism Studies

	Bulk Slag Mass Transport	Gas Slag Reaction	Transport in Halo	Gas Metal Reaction	Observed Swelling?	Slag Boundary Layer transport?	Droplet C Diffusion	Rate Controlling Step
Mulholland [5]	●	●	●	●				Possibly halo diff.
Min & Fruehan [6]	●	●	●	●			●	Mixed Ctrl: -FeO trans. -halo diff. -gs. Mt. rx
Murthy et al [8, 9]	●	●	●	●	Possibly: change in mechanism noted	●	●	-FeO trans. -halo diff.
Gare & Hazeldean [11]	●	●	●	●	●			
Molloseau & Fruehan [13]	●	●	●	●	●		●	
Chen & Coley[19,20]	●				●	●	●	Nucleation of internal CO

2.4 Nucleation of CO Bubbles in Liquid Fe-C

A kinetic model to explain the results was subsequently developed by Chen[19]. The model involved the use of Kwak and Oh's clustering process[22] involving the formation of metastable CO clusters:

$$\underline{C} + \underline{O} \rightarrow C^* + O^* \rightarrow (CO)^* \tag{2.22}$$

with C*, O* and CO* representing metastable clusters. As observed by other researchers[8,9], the calculated supersaturation pressure was orders of magnitude too large to support the observed nucleation rates[19]. Another CO nucleation rate was developed according to[37]:

$$J_s = N_O \exp\left(-\frac{\Delta H}{RT}\right)\left(\frac{3\sigma}{\pi m}\right)^{1/2}\exp\left(-\frac{16\pi(\sigma)^3}{3kT\left[P_{v,e}-P_L\right]^2}\right) \tag{2.23}$$

where N_O is the number concentration of CO embryos in the droplet, ΔH is the enthalpy of formation for 1 CO molecule, σ is the metal-gas surface tension, m is the mass of one molecule, P_{ve} is the pressure in the vapour bubble at equilibrium, P_L is the pressure in the liquid (ferrostatic), and k is Boltzmann's constant. The observed nucleation rate was essentially zero[19]. This is inconsistent with the observations of significant swelling observed in practice, so a surface tension modifying factor ,Ψ, was added to fit the data[19]:

$$J_s = N_O \exp\left(-\frac{\Delta H}{RT}\right)\left(\frac{3\boldsymbol{\Psi}\sigma}{\pi m}\right)^{1/2}\exp\left(-\frac{16\pi(\boldsymbol{\Psi}\sigma)^3}{3kT\left[P_{v,e}-P_L\right]^2}\right) \tag{2.24}$$

Several suggestions have been put forward in an effort to understand the discrepancy necessitating the use of the parameter Ψ. A common suggestion is that the application of macroscopic surface tension values to gas embryos that could be extremely small is an invalid assumption[23].

Tolman[24] put forth a model in the 1940s to explain the effect of small radii on surface tension. Beginning with the Gibbs isotherm,

$$d\sigma = -\Gamma d\mu \tag{2.25}$$

where Γ is the superficial density of material at the interfacial boundary, μ is the chemical potential of the surface species. Coupling equation (2.25) and the well-known Laplace expression, a derivation is made to approach the small scale behaviour[24]. In the end a parameter δ is introduced. The parameter δ represents the distance from the interface of an imaginary surface which makes the superficial density Γ (surface density of surface active element) diminish when computed with respect to δ[24]. The obtained and simplified expression is[24]:

$$\frac{\sigma}{\sigma_o} = \frac{1}{1+\frac{2\delta}{r}} \tag{2.26}$$

with σ being the applicable surface tension and σ_o being the macroscopic surface tension. Table 2.2 shows the calculated results from Tolman showing the depression of ratio $\frac{\sigma}{\sigma_o}$ [23]

:

Table 2.2: Results from Tolman. Source: [23]

δ/r	σ/σo	δ/r	σ/σo
0	1	0.4	0.52
0.01	0.98	0.5	0.46
0.02	0.96	0.6	0.41
0.05	0.91	0.7	0.36
0.1	0.83	0.8	0.33
0.2	0.70	0.9	0.30
0.3	0.60	1.0	0.28

Another possibility, is the presence of double charged surface adsorbed oxygen ions[25-26]. In his paper[25], Levine suggests that the typical expression for free energy of formation of a vapour nucleus be modified to include the surface energy "absorbed" by the presence of O^{2-} ions, σ_o. The Laplace equation is subsequently modified[25], and as a final the effective surface tension of the vapour nuclei are seen to decrease due to the energy associated with the presence of the oxygen ions. While the range of values of δ/r are still larger than those needed to support the nucleation rates observed in Chen's study[19] and the present study, it does illustrate the possibility of embryo size influencing the interfacial tension.

Robertson and Jenkins[27] suggest the possibility that turbulence at the droplet surface produces turbulence in the melt which sweeps gases or slag particles into the droplet acting as nucleation points.

Bowers *et al.*[28] suggest an alternative possibility whereby a "uniform dissolved gas blob" which has a uniform but slightly elevated gaseous concentration grows by random fluctuations until its Helmholtz energy permits the transformation to a bubble[28]. Since it is merely a diffuse region of elevated gas concentration, surface tension effects would be expected to be negligible during its growth[28].

2.5 Summary

Numerous studies have been carried out regarding droplet residence time, generation rate and decarburization rate. In general two decarburization reaction regimes are reported: an external "halo" reaction at the droplet surface and internal reaction below the droplet surface.

As X-Ray visualization became available over the years more detailed studies on the swelling of droplets were made possible. The interaction between droplet generation rate, residence time and decarburization rate is seen to be increasingly present and necessary for a thorough understanding of the decarburization process in slags.

Chapter III

Experimental Apparatus

The experimental apparatus used in this study was the same as that developed and successfully implemented by Chen[19,20]. In a broad sense, there are two complementary components in the experiments: slag-metal reaction rate measurements by a constant volume pressure increase technique and visualization of the reactions by X-Ray video imaging. One major difference is that in the case of the former study[19,20], the X-Ray imaging was used primarily to observe droplet swelling rates, while in the present study the its primary use was to observe whether carbon boil takes place and in that case, the time before the onset of internal nucleation.

3.1 Kinetic Measurements

3.1.1 Reaction Rate Measurements

A constant volume pressure increase (CVPI) technique was utilized to measure the gas evolution from the slag-metal reactions with time. The experiments require a well sealed reaction chamber with a differential pressure transducer (FLW Southeast Inc., 157C-W050NR, Very Low Pressure Transducer). Evolution of CO gas from the reactions results in an increase in pressure proportional to moles of gas released. Data from the pressure transducer is recorded by computer software (via a RS232 Interface) at a selected frequency, which was 1 Hz in the case of this study. Pressure transducer output (differential pressure in pounds per square inch) was measured. Measurements

can be made with rated accuracy up to 2 PSI above the STP atmosphere. Figure 3.1 shows an example output (adjusted from PSI to moles CO) from a CVPI experiment.

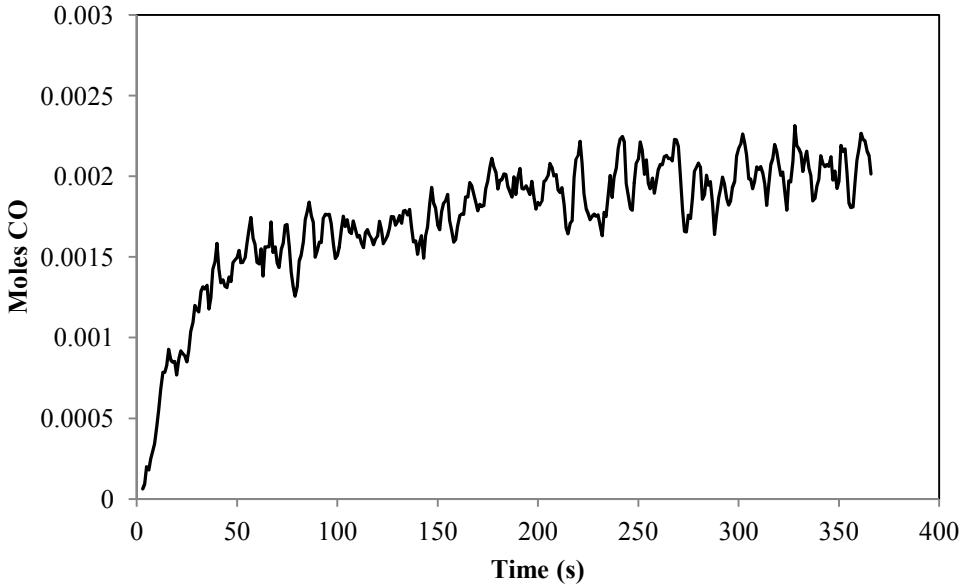

Figure 3.1: Typical pressure transducer output.

3.1.2 Calibration of the Pressure Transducer

After any change in experimental setup (crucible size change, change in support mechanism), a new calibration of the pressure transducer has to be carried out. This requires that the furnace be brought to the temperature of interest for the experiments. Inert gas is subsequently injected into the furnace with a syringe in known quantities, generally 10 mL to 20 mL. The exact time of each injection was noted. It was found during the course of the experimental program that it takes a certain time (around 30 seconds) for the pressure reading to reach a stable unchanging value. The requirement

for this waiting period is due to warming of the injected gas from room temperature to the furnace temperature. This warming is accompanied by an isometric increase in pressure.

In order to ensure that no heating effects of the gas were included in the calibration curves, a gap of 4 minutes was implemented between injections. This ensured two things: certainty that heating of the gas does not influence the calibration curve, and certainty that the furnace was well sealed. The use of argon gas instead of air for the calibrations as was the case with Chen's experiments[19,20] enabled same-day calibration curves to be determined for each experiments. It was found that a very high reproducibility existed between experiments with the same apparatus (support mechanism configurations, crucible diameters and large protective crucible diameters). A line can be fitted to the calibration curve of the form

$$y = \alpha x \tag{3.1}$$

where α (mol / PSI) relates the measured pressure change to moles of gas released (injected in the case of the calibration and evolved in the case of the kinetic measurements). In other words,

$$\alpha = \frac{\partial n_{CO}}{\partial P_{measured}} \tag{3.2}$$

An example of a typical calibration curve is presented in Figure 3.2.

Since three different configurations were used over the course of the experimental studies, at least three calibrations needed to be undertaken. The term "configurations" corresponds here to different permutations of inner crucible size, outer crucible size and structural support ceramics within the furnace.

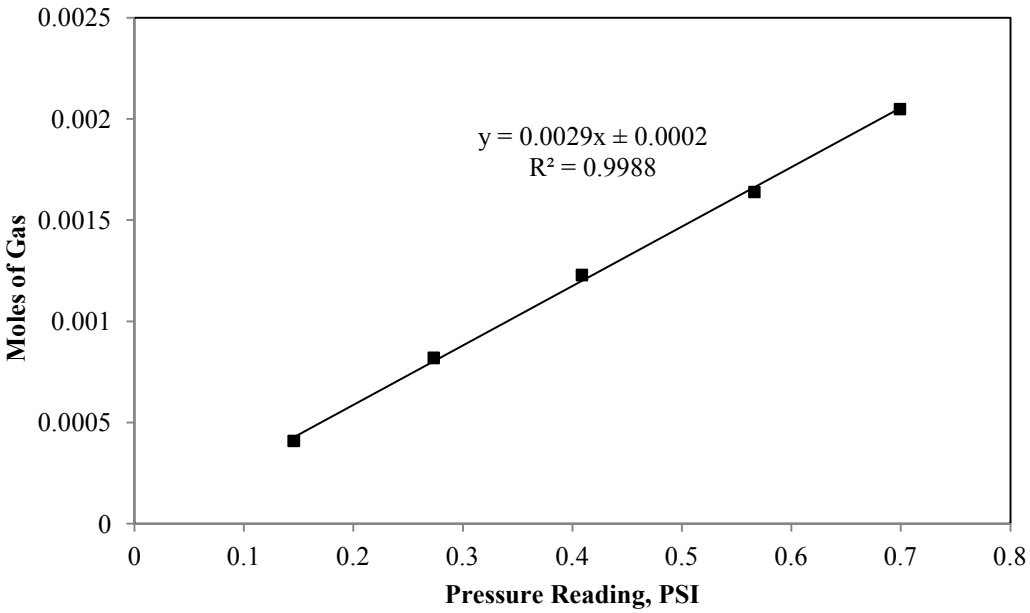

Figure 3.2: Typical calibration curve at T = 1500°C.

Table 3.1 gives these values for the temperature of interest (T = 1500° C).

Table 3.1 : Pressure Transducer Calibration Constants at T = 1500°C

Configuration	α (mol / PSI)
"A"	0.0036
"B"	0.0029
"C"	0.0028

3.2 Material and Chemical Preparation

3.2.1 Alloy Preparation

Fe-C-S alloys were prepared by mixing pure electrolytic Fe, laboratory grade high purity graphite powder and ferrous sulphide, FeS in an alumina crucible (McDanel, O.D. = 1.375", Height = 1.5"). Although it is expected from iron-carbon equilibria that a liquidus would form at lower temperatures than 1538° C, premelting was performed at 1550° C to ensure melting of all electrolytic iron and dissolution of the graphite in the liquid. The materials used in preparing the alloys are outlined in Table 3.2

Table 3.2 : Materials Used in Preparation of Alloys

Material	Supplier	Purity
Electrolytic Iron	Unknown	>99%
Graphite Powder	Alfa Aesar	>99%
Ferrous Sulphide	Fisher Chemicals	>99%

Experience in previous studies[19,20] and the present study show that not all graphite measured before melting is accounted for in the final chemistry analysis of the prepared alloys (yield loss). Thus a slightly larger quantity of graphite powder than desired in the final chemistry is added to the crucible before melting. Qualitative experience in the preparation of alloys for the present study showed that a yield loss in carbon of 8 – 12 % by mass is typical. Similar yield losses were observed for calculated

required FeS additions. It is not expected that this yield loss is due to oxidation of the dissolved carbon by contaminate gaseous oxygen since the loss decreased significantly when graphite powder was placed at the bottom of the crucible with iron forming a thick layer above. This suggests that the observed C yield loss is attributable to fine graphite powder being physically lifted out of the crucible by moving argon.

Mixtures of premeasured electrolytic iron and graphite powder were left in the furnace and heated to 1550° C overnight in a high purity argon atmosphere (Alphagas). Ensuring that the mixture had been at the constant temperature for at least an hour, samples were pipetted out in a quartz tube (I.D. = 5 mm) and immediately quenched. Droplets were created by sectioning into pieces of appropriate mass. No droplets were sectioned from within 2 cm of the exposed end. Calculation for the diffusion of oxygen into the alloy between suction and quenching shows the diffusion distance attained to be less than 5 mm (for liquid iron) and less than 2 mm (for γ iron). As oxygen content was an important experimental parameter, an analysis of the oxygen exposure of the alloys during the process is conducted in the Appendix.

A modification on the apparatus of Chen was carried out whereby an inner alumina delivery tube was held directly above the crucible and topped with a removable cap. Premelting of graphite and electrolytic iron was carried out overnight and the first suctioning of 0 % S hot iron was made. Ferrous sulphide could be introduced through the inner alumina tube by means of increasing the shielding argon flow (to ensure positive pressure at all times), removing the sealed cap on the inner tube and dropping a premeasured mass of FeS into the melt. After waiting 2 to 3 hours for homogenization,

another sample could be taken with a higher FeS content and more FeS introduced if necessary. By this means droplets with constant carbon content and varying sulphur content could be achieved.

3.2.2 Slag Preparation

Slags were prepared by mixing high purity SiO_2, CaO, MgO and FeO powders. Ball milling for at least 5 minutes was used to low particle size, ensure a high degree of mixing of the powder and higher random surface contact between the various species. Previous studies[9,16,17] found that prefusion of the slags was unnecessary, particularly as there is no slag-metal contact before the reactions in the current experimental setup.

Prior to preparation of the slags, the SiO_2, CaO and MgO powders were heated in a furnace and held at 500° C for three hours to drive off any bound moisture. This is a particular concern in the case of CaO. Dried powders were subsequently kept in a sealed dessicator to prevent rehydration before measurement. The FeO was not dried prior to measurement since this would expose it to air at high temperature for a prolonged period of time. Since the FeO was supplied packed under argon and was always packed under argon between uses in the laboratory, it is expected that any hydration from the atmosphere would be negligible. Table 3.3 summarizes the materials used in preparation of the slags.

Table 3.3 : Materials Used in Preparation of Slags

Material	Supplier	Purity
SiO_2	Alfa Aesar	>99.5%
CaO	Alfa Aesar	>99%
MgO	Fisher Chemicals	>99%
FeO	Alfa Aesar	>99.5%

3.3 High Temperature Apparatus

3.3.1 Furnace Setup

The furnace used in the present study is heated by four molybdenum disilicide elements. Two type B thermocouples were connected to a EUROTHERM programmable controller. As described by Chen[19,20], two rectangular holes are cut out of the outer steel casing of the furnace as to allow X-Ray penetration for imaging of the slag-metal reactions.

The inside of the furnace contains an alumina tube (I.D. = 3.0", O.D. = 3.5" Height = 30") sealed with O-Rings and stainless steel end fittings. This tube was the sealed pressure system for the CVPI measurements. Water cooling was provided at the steel end caps to prevent O-Ring melting. The crucible was magnesium oxide with two sized crucibles used (due to availability, not experimental necessity). The two sized crucibles used were (O.D. = 1.75", height = 3") and (O.D. = 1.375", height = 2.5"). It was found that in the case of the smaller diameter crucible there was a higher probability of

subsequent droplets falling a previously reacted droplet at the bottom, so in some cases only 2 or 3 experiments could be conducted in one run with the smaller crucibles, versus 4 with the larger crucibles.

An alumina dispensing tube was used to guide the droplet into the furnace. Upon falling, the droplet would stop above a small hole (3/16" diameter) at the bottom of the tube and melt. Following melting, the droplet could fall through the hole into the molten slag.

While in operation the furnace was flushed continuously with high purity "Alpha Gas" argon . The argon passed through a column of scrubbing Drierite before entering the furnace.

A calibration in temperature is required in the furnace as the thermocouples connected to the controller are not located directly in the alumina working tube, rather on the opposite side. The calibration is also necessitated by the gradient in temperature along the height of the working tube. Figure 3.3 shows the calibration curve near the furnace centre .

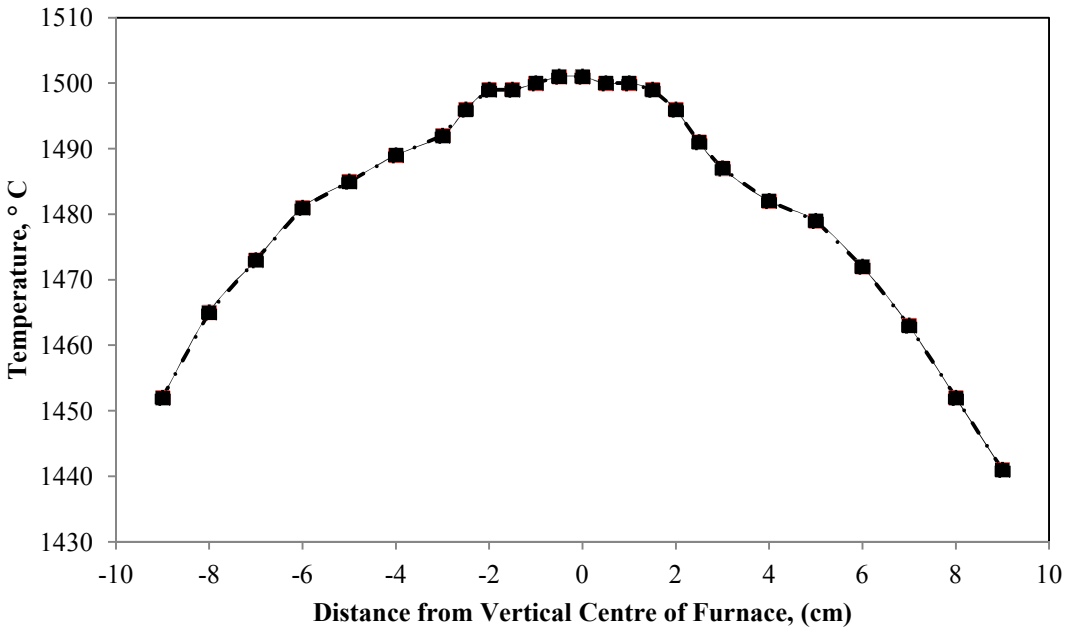

Figure 3.3: Temperature calibration for furnace setting of 1509°C corresponding to experimental condition of 1500° C.

It is seen that for a temperature accuracy of ±5 °C, the zone about the centre is around 5.5 cm in height while for ±1 °C, the zone is about 3.5 cm in height. The temperature profiles were taken with the definition of furnace centre as the centre of the alumina cut out from a vertical orientation.

The overall setup of the apparatus designed by Chen[19, 20] and modified slightly for the current study is presented in Figure 3.4.

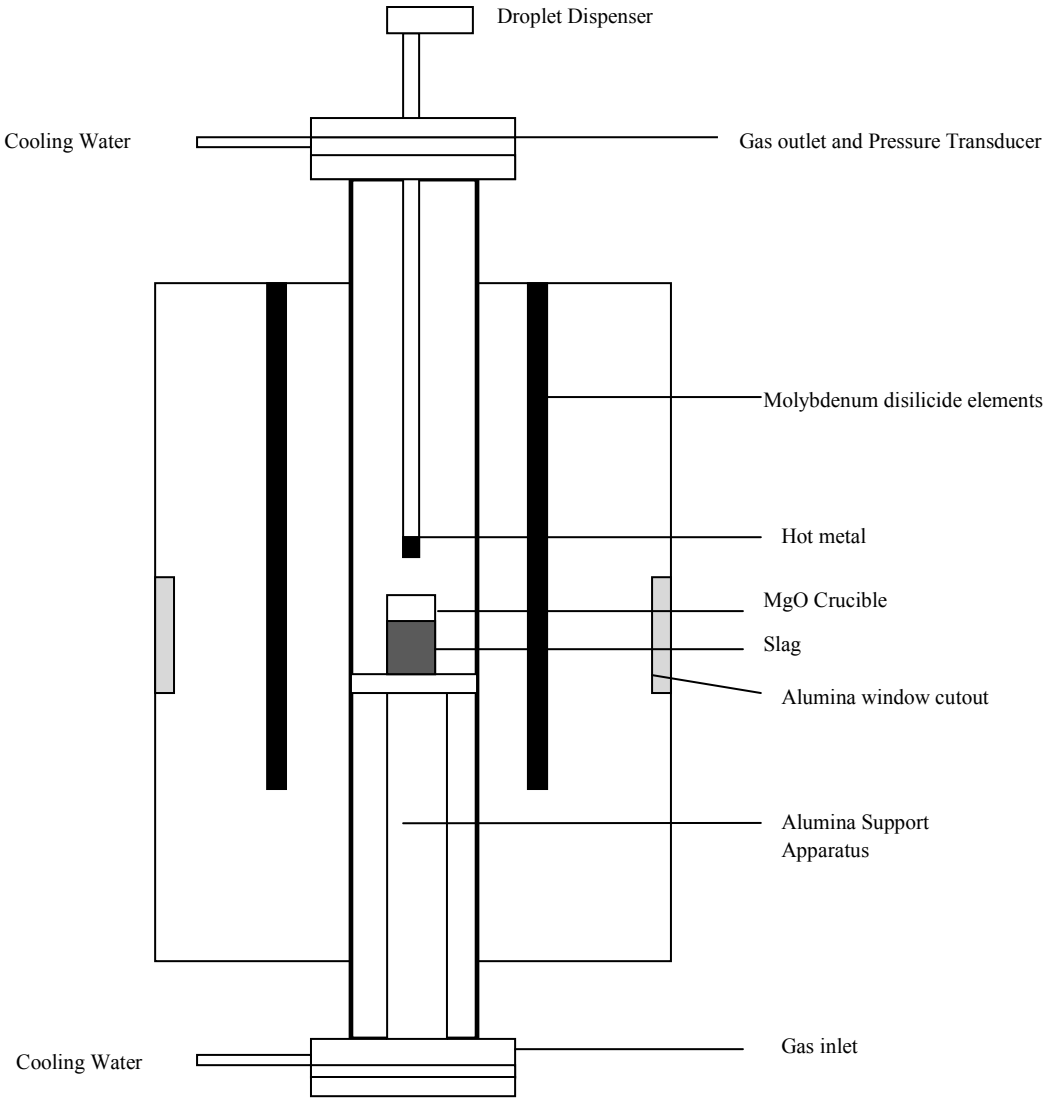

Figure 3.4: Overall view of the furnace setup

Chapter IV

Results, Numerical Model Development and Discussion

4.1 Experimental Results

4.1.1 General Slag-Metal Reaction Observations

Over the course of an experiment, several reaction behaviours were observed. Most of the experimental conditions considered in this study produced droplet swelling. The carbon boil behaviour was observed in droplets in all experimental conditions considered in this study, with the exception of low sulphur droplets in slags of low FeO content.

In droplets where a carbon boil was observed, the droplets would fall into the slag and an external reaction period was initiated immediately in all cases. Bubbles could be observed leaving the droplet surface with the highest gas density directly adjacent to the surface, giving the appearance of a halo. During this period, the droplet was observed to remain of constant diameter with no measureable swelling. This external decarburization period could last in duration from very negligible times, less than 0.13 seconds, to several seconds depending on the experimental conditions considered. The droplet was then observed to swell, with droplet diameters expanding to 1.4 to greater than 3.6 times the original diameter. In some cases the droplet would float above the slag in a foam for several seconds before falling to the bottom of the crucible. The droplet could also float at the slag surface for several seconds.

In a few experiments, no carbon boil was observed. In this situation the droplet would fall into the slag and the reaction at the surface was immediately initiated creating bubbles. The droplet would be observed to slowly descend to the bottom of the crucible, where it would continue to react at its surface.

Internal swelling was observed across a broad range of experimental conditions. Due to experimental constraints and availability, experiments were conducted at only one temperature, 1500°C.

The experiments conducted were designed to span a range of starting carbon contents from approximately 4.2% to 2.5%. Sulphur contents spanned from 0 to approximately 0.10 %. The range for slag FeO content was 8.5 to 30 percent at a constant CaO / SiO2 of 1.2 and MgO at 12%.

The general sequence of the progress of experiments is presented in Figure 4.1 a – d.

Chen[19] presented results at mostly lower carbon contents (2.5 to 2.9 %), so the emphasis of this experimental program was to characterize behaviour at higher carbon contents (approximately 4.2%).

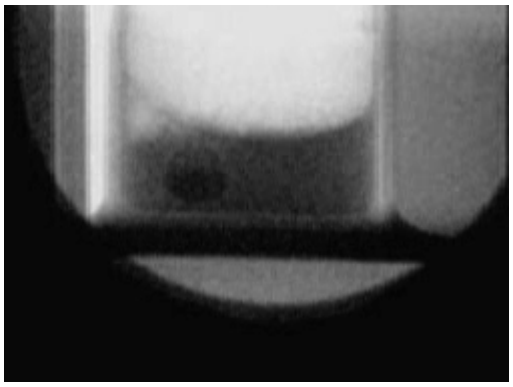

a. Droplet arrives in slag

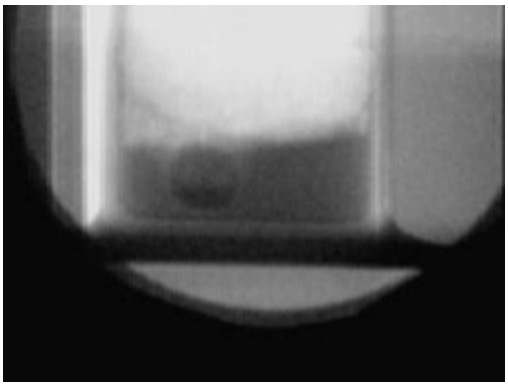

b. Droplet begins to rise. Some swelling evident.

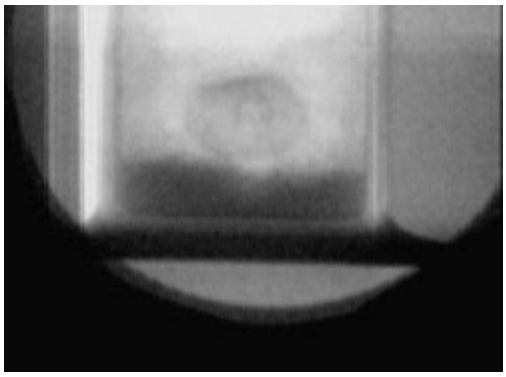

c. High degree of droplet swelling. Droplet may rise into slag foam.

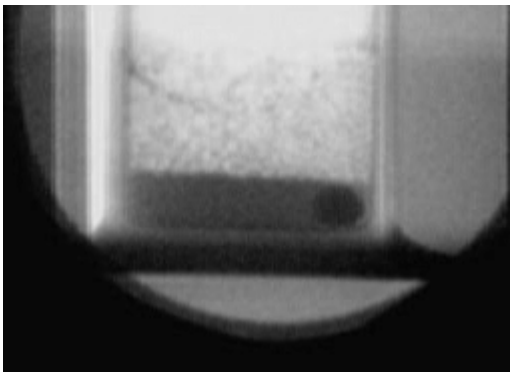

d. Droplet settles into slag. Little activity evident.

Figure 4.1 Snapshots of general reaction progress for 1.0 g droplet in FeO = 30 % slag.

4.1.2 Effect of Slag FeO Content at Higher Carbon

A set of experiments was designed to quantity the effect of slag FeO contents, with tests at 8.5, 12, 15, 25 and 30% FeO by weight. The results are shown in Figure 4.2. At 0.007% S, droplet swelling was observed at all FeO contents starting at 8.5%. All droplets in the series contained 4.254% C, had mass of 1.33 g and experiments carried out at 1500°C. It is seen that the availability of oxygen is an important factor driving the gas evolution.

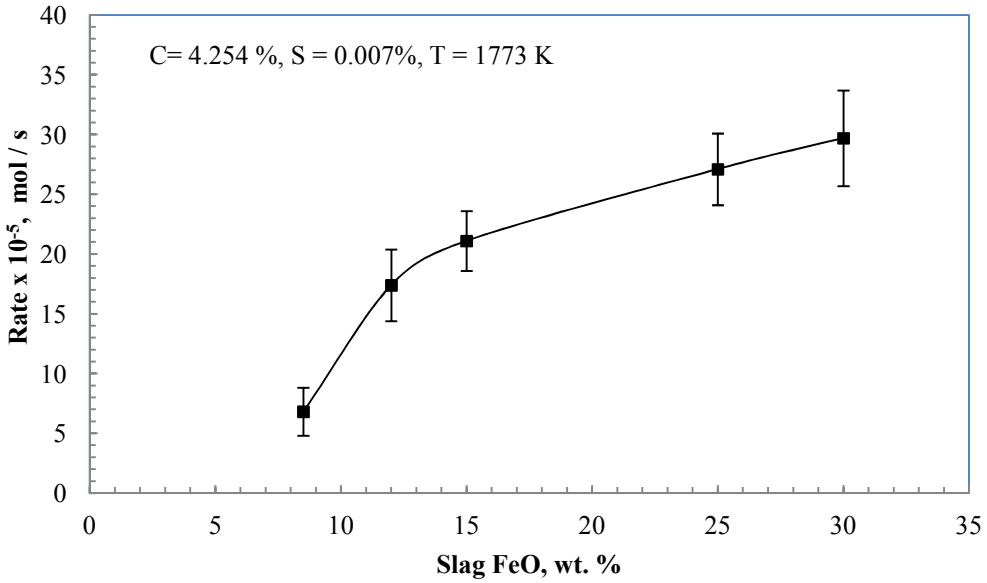

Figure 4.2: Variation of CO evolution rate with slag FeO content

4.1.3 Effect of Droplet Mass

Another set of experiments was designed to view the variation in evolution rate with varying droplet mass. Droplet C, slag FeO, S and basicity were held constant and

mass varied by using different masses of the same prepared alloy. It is seen that at elevated carbon contents, a strong linear dependency of the rate on mass (volume) exists. Figure 4.3 shows relationship of rate and droplet mass. Extrapolation of the experimental data is seen to extend through the origin.

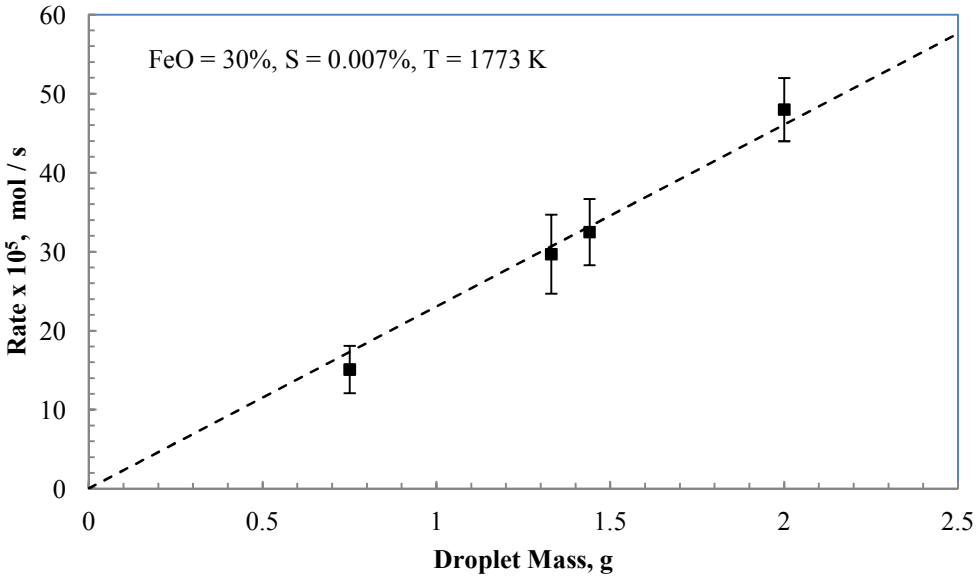

Figure 4.3: Variation of CO evolution rate with droplet mass with 4.254% C droplets.

4.1.4 Effect of Sulphur Content

The sulphur content of droplets was varied holding other parameters constant in a 20% FeO slag. The rate with sulphur as in the case of Chen's results is observed to pass through a maximum somewhere between 0.005 and 0.019 % S. The results are presented in Figure 4.4. Sulphur contents indicated as 0% in this study are S < 0.001 %.

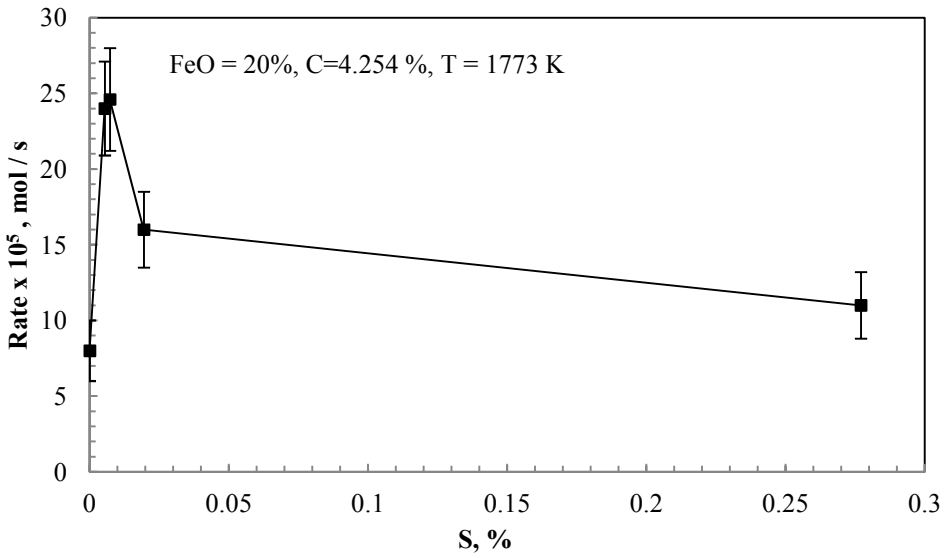

Figure 4.4: Variation of CO evolution rate with S in 4.254% C droplets.

4.1.5 No Droplet Swelling

In some cases no internal evolution of gas was observed. The reaction took the appearance of a "gas halo" surrounding the droplet as it slowly descended through the crucible. In particular this behaviour was evident in lower FeO content slags (always less than 12 % FeO) in droplets where sulphur contents were low (less than 0.007%) or droplet masses were high. Table 4.1 summarizes the results of all runs in this experimental program indicating conditions where no internal nucleation of gas was observed to take place.

Table 4.1: Experimental conditions with no carbon boil observed.

FeO (%)	C (%)	S (%)	Droplet Mass (g)
8.5	4.254	0	1.0
8.5	4.254	0.0072	2.0
8.5	2.573	0	1.0
12.0	4.254	0	2.0

4.1.6 Experimental Conclusions

In higher C droplets (~4.2 % C) at 1773 K:

1. A strong dependency upon slag FeO content is observed with evolution rates increasing as much as 6 fold between 8.5 % and 30 % FeO.

2. The reaction rate is observed to increase linearly with droplet mass.

3. A maximum in rate is observed between 0.005 and 0.019 wt % S.

4. At low slag FeO contents (12% or less) at low S concentrations (0 %, or 0.007 % when droplet mass is higher at 2.0 g), no carbon boil was observed

4.2 Numerical Model Development

4.2.1 Model Formulation

For a droplet containing no dissolved oxygen, there is an initial incubation period before the onset of internal CO evolution. This period corresponds to the diffusion of oxygen into the droplet and also involves the reaction at the surface, where there exists a ready supply of oxygen from the slag to drive the external decarburization. Therefore oxygen diffusing into the droplet is the balance of oxygen supply (from the slag) and external reaction (producing CO).

A model incorporating the external decarburization reaction, slag oxygen supply, and the balance diffusion into the droplet was developed by Sun[14]. As a result, a framework for the diffusion of FeO in the slag, dissociation of FeO at the surface, decarburization at the surface, C diffusion in the droplet and O diffusion in the droplet already exists.

The model by Sun[14] is therefore taken as a guide for governing equations for the external decarburization regime. The results from Sun's numerical framework are then applied to the internal decarburization model developed by Chen[19,20] to determine when the appropriate conditions for internal nucleation are obtained.

Transport of FeO in the slag is calculated assuming that boundary layer theory can be applied[14] according to

$$J_{FeO} = -\frac{d(FeO)}{dt} = \frac{Am_s\rho_s}{100M_{FeO}}\left[(FeO)_{r0} - (FeO)_{bulk}\right] \qquad (4.1)$$

where J_{FeO} is the flux of FeO given in mol / s, A is the droplet-slag interfacial area, m_s is the mass transport constant of FeO in the slag, $(FeO)_{r0}$ is the concentration of FeO at the interface given in wt. % and $(FeO)_{bulk}$ is the bulk FeO concentration. A is given in cm^2 and m_s is given in cm/s.

The surface adsorption reaction

$$(FeO) = Fe + \underline{O} \tag{4.2}$$

is assumed by Sun[14] to proceed quickly and therefore be in local equilibrium at the interface. Sun's model however does not consider sulphur as a surface active element which would block potential adsorption and reaction sites for the oxygen. The surface sulphur will lower the effective area at which oxygen adsorption can occur. Therefore the surface sulphur prevents the slag adjacent to the interface from reaching local equilibrium with the dissolved oxygen at the droplet side of the interface.

The fraction of surface sites occupied by sulphur, θ_s , can be obtained by combining the Gibbs and Langmuir isotherms as discussed by Belton[29] according to

$$\theta_s = \frac{K_s a_s}{1+K_s a_s} \tag{4.3}$$

where a_s is the activity of the sulphur and K_s is the adsorption coefficient for the sulphur. The variation of K_s in Fe-C-O-S melts is suggested[30] (for S activities, rather than as tabulated for weight percent as by Sain[31]) to vary according to

$$\log(K_s) = \frac{9960}{T} - 2.75 \tag{4.4}$$

If local equilibrium cannot be established at the surface due to surface sulphur, then equation 4.1 for J_{FeO} must also be equal to

$$J_{FeO} = \vec{k}A(1-\theta_s)a_{FeO}^{r0} - \overleftarrow{k}A(1-\theta_s)h_O^{r0} \quad (4.5)$$

where a_{FeO}^{r0} is the activity of iron oxide adjacent to the interface, h_O^{r0} is the activity of oxygen at the interface, $\vec{k}$ is the forward rate constant for adsorption of O at the interface (forward rate constant for equation 4.2), $\overleftarrow{k}$ is the rate constant for the reverse reaction. Since $\vec{k}$ and $\overleftarrow{k}$ are related to the equilibrium constant for equation 4.2 according to

$$K = \frac{\vec{k}}{\overleftarrow{k}} \quad \text{then}$$

$$J_{FeO} = \vec{k}A(1-\theta_s)\left[a_{FeO}^{r0} - \frac{h_O^{r0}}{K_{Fe}}\right]$$

As $a_{FeO}^{r_0} = \gamma_{FeO}^{r0}X_{FeO}^{r0}$, with γ_{FeO}^{r0} being the activity coefficient of FeO at the slag-metal interface and X_{FeO}^{r0}being the mole fraction of FeO at the interface,

$$J_{FeO} = \vec{k}A(1-\theta_s)\left[\gamma_{FeO}^{r0}X_{FeO}^{r0} - \frac{h_O^{r0}}{K_{Fe}}\right] \quad (4.6)$$

Equations 4.1 and 4.6 are solved simultaneously to determine concentration of FeO adjacent to the interface based on the results of the previous iteration in time. Appropriate conversions between weight percentage and mole fractions were made and use was made of a reported correlation[32] for γ_{FeO}^{r0}.

The surface reaction rate is calculated according to the framework suggested by Sun[14] and modified for surface reaction site availability

$$J_r = -\frac{\partial N_{CO}}{\partial t} = (1-\theta_s)\frac{Ak_r}{100M_C}\left[h_O^{r_0}h_C^{r_0} - \frac{P_{CO}^{r0}}{K_C}\right] \quad (4.7)$$

where k_r is the rate constant at the surface in mol cm^{-2} s^{-1}, $h_i^{r_0}$ represents activity of a species at the surface, P_{CO}^{r0} represents partial pressure of CO and K_C is the reaction equilibrium constant for reaction (2.1).

Since carbon does not accumulate at the surface, by a simple mass balance the stoichiometric equation relating flux of C towards the surface J_C and surface reaction rate J_r as given by Sun is

$$J_C = J_r \quad (4.8)$$

Likewise a balance in oxygen gives

$$J_{FeO} = -J_r + J_O \quad (4.9)$$

for relating the flux of FeO, J_{FeO}, reaction rate and flux of oxygen J_O into the droplet.

The rate of diffusion of carbon to the surface is given by[14]

$$J_C = \frac{AD_C\rho_m}{100M_c dr}\left([C]^{r0-dr} - [C]^{r0}\right) \quad (4.10)$$

where D is the diffusion coefficient in cm^2 / s , dr is the discretized differential radial distance, $[C]^{r0-dr}$ is the concentration of Carbon at one discretized differential radial

distance from the surface and $[C]^{r0}$ is the concentration of C at the surface. Likewise oxygen diffusion into the drop is given by[14]

$$J_O = \frac{AD_O\rho_m}{100M_O dr}\left([O]^{r0-dr} - [O]^{r0}\right) \tag{4.11}$$

The equilibrium constant for CO decarburization is required as is it appears in equation (4.6) to determine the driving force for suface reaction. This is equal to

$$K_C = \left(\frac{P_{CO}}{h_c h_O}\right)_{equilibrium} \tag{4.12}$$

where h_O represents the activity of oxygen and h_c the activity of carbon. The activities of C and O can be calculated according to

$$h_C^{r0} = f_C^{r0}[C]^{r0} \tag{4.13}$$

$$h_O^{r0} = f_O^{r0}[O]^{r0} \tag{4.14}$$

$$\log f_C = e_C^C[C]^{r0} + e_C^O[O]^{r0} + e_C^S[S]^{r0} \tag{4.15}$$

$$\log f_O = e_O^C[C]^{r0} + e_O^O[O]^{r0} + e_O^S[S]^{r0} \tag{4.16}$$

where f_i^{r0} is the activity coefficient of a species, and e_i^j is the interaction coefficient between species i and j. The interfacial quantities are determined by simultaneous solution of the above relations given the results of the previous iteration in time (or the initial conditions in the case of the first iteration).

Diffusion is assumed to occur in a one dimensional fashion in the radial direction of the droplet. This is due to the symmetry The variation in composition of C and O in the droplet are determined by Fick's second law in spherical coordinates for one dimension according to

$$\frac{\partial[\mathrm{C}]}{\partial \mathrm{t}} = \frac{\mathrm{D_C}}{\mathrm{r^2}} \frac{\partial}{\partial \mathrm{r}} \left[\mathrm{r}^2 \frac{\partial[\mathrm{C}]}{\partial \mathrm{r}} \right] \tag{4.17}$$

and

$$\frac{\partial[\mathrm{O}]}{\partial \mathrm{t}} = \frac{\mathrm{D_O}}{\mathrm{r^2}} \frac{\partial}{\partial \mathrm{r}} \left[\mathrm{r}^2 \frac{\partial[\mathrm{O}]}{\partial \mathrm{r}} \right] \tag{4.18}$$

which can be discretized according to

$$\frac{\mathrm{C_{i,j+1}} - \mathrm{C_{i,j}}}{\Delta \mathrm{t}} = \mathrm{D} \frac{\mathrm{r_{i+0.5}^2} \frac{\mathrm{C_{i+1,j}} - \mathrm{C_{i,j}}}{\Delta \mathrm{r}} - \mathrm{r_{i-0.5}^2} \frac{\mathrm{C_{i,j}} - \mathrm{C_{i-1,j}}}{\Delta \mathrm{r}}}{\mathrm{r_i^2} \Delta \mathrm{r}} \tag{4.19}$$

In this case $C_{i,j}$ represents the concentration of a species with i being the spacial mesh index and j being the time step index. Δr is the radial discrete step Δt is the discrete time step. Calculations were subject to the condition for numerical stability of

$$\Delta \mathrm{t} \ll \frac{\Delta \mathrm{r}^2}{2\mathrm{D}} \tag{4.20}$$

The model for nucleation by Chen[16,17] is simultaneously applied to determine the expected internal nucleation rate. The internal nucleation of CO bubble is expressed quantitatively by

$$\mathrm{J_{CO}} = \mathrm{N_O} \exp\left(\frac{-\Delta \mathrm{H}}{\mathrm{kT}}\right) \left[\frac{3\Psi\sigma}{\pi \mathrm{m}}\right]^{\frac{1}{2}} \exp\left[\frac{-16\pi(\Psi\sigma)^3}{3\mathrm{kT}[\mathrm{P_{ve}} - \mathrm{P_L}]^2}\right] \tag{4.21}$$

With N_O the number concentration of embryos in the liquid, σ being the surface tension at the interface, ΔH being the heat for forming one CO embryo, m being the mass of one CO embryo, k being the Boltzmann constant, T being the absolute temperature, P_{ve} being the equilibrium vapour pressure and P_L being the surrounding liquid pressure. and Ψ being the surface tension modifying parameter.

J_{CO} gives rate of formation of critically sized embryos in embryos / m^3 s. Therefore the creation of one critically sized nucleus is given subject to the condition

$$\int_0^t \int_0^R J_{CO}(r,t)\, A(r) dr\, dt = 1 \qquad (4.22)$$

The timestep at which 1 critically sized nucleus is taken as the time to the onset of internal CO nucleation. This could have been defined by an arbitrary nucleation rate CO, but by defining the creation of 1 critically sized nucleus as the criterion, good agreement with the experimental results were obtained. This choice of criterion is also justified by the subsequent rapid increase in nucleation rate if the model were left running under the external reaction/diffusion regime. Figure 4.5 illustrates an example of this "embryo explosion".

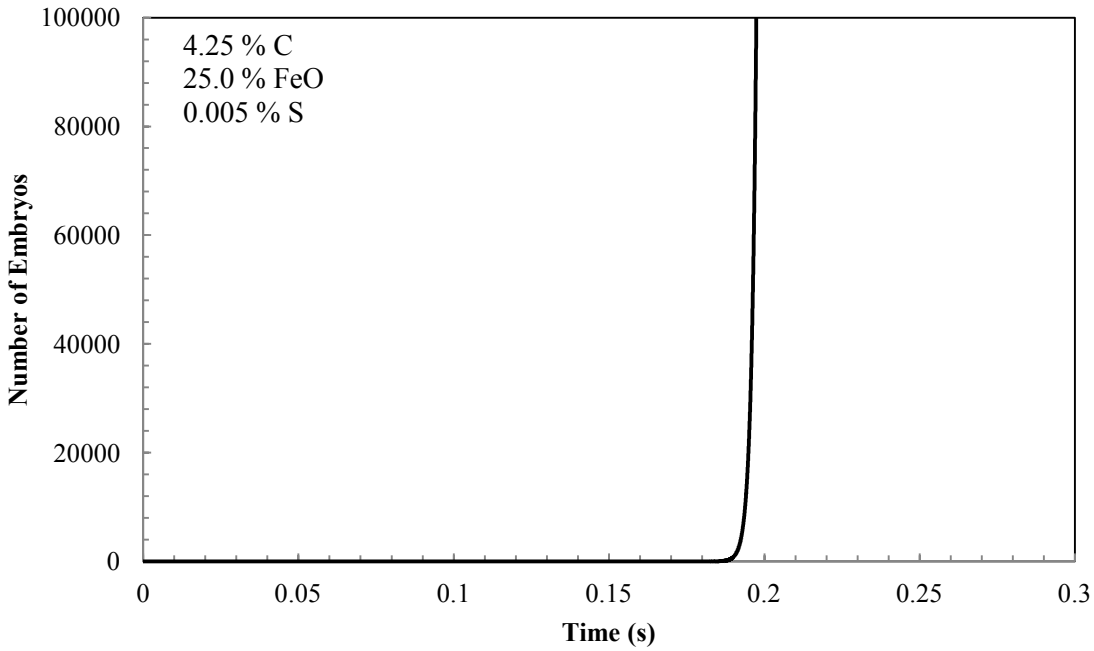

Figure 4.5 Typical example of a calculated "embryo explosion".

4.2.2 Model Input Data

Input thermodynamic, chemical and kinetic data was drawn from many sources. In many cases the input data was the same as recommended by Sun in his modelling study[14]. Data in relation to the internal nucleation of bubbles was drawn from the previous work by Chen[19,20] and the current study. Table 4.2 summarizes the data used to perform model calculations.

Table 4.2 Input Data used in Computation

Parameter	Description	Worker	Values
D_O	Oxygen Diffusion Coefficient (cm^2 / s)	Heisterkamp and Lohberg[33]	$5.1x10^{-3}\exp(-\frac{6083}{T})$
D_C	Carbon Diffusion Coefficient (cm^2 / s)	Kowakami et al[34]	$7.4x10^{-3}\exp(-\frac{5891}{T}$
Interaction coefficients eoc, etc.	Interaction coefficients	Steelmaking Data Sourcebook [35]	Typical tabulated values.
m_{slag}	Mass transport rate coefficient of "FeO" in slag (cm / s)	Min and Freuhan[6]	0.005
k_r	Rate coefficient for decarburization reaction (g / cm^2 s)	Sibata, Sun, Mori[36]	0.136
γ_{FeO}	Activity Coefficient of slag FeO	Basu, Lahiri and Seethamaran[32]	$\log(\gamma_{FeO}) = -0.7335\log(X_{FeO}) - 0.2889$
K_C	Eq'm constant for the decarburization reaction, equation (4.12)	Steelmaking Data Sourcebook [35]	$\log(K_C) = \frac{1160}{T} + 2.003$
K_{Fe}	Eq'm constant for dissociation reaction, equation	Steelmaking Data Sourcebook [35]	$\log(K_{Fe}) = \frac{6150}{T} - 2.604$
Ks	Sulphur adsorption coefficient	Jimbo, Sharon and Cramb [30]	$\log(K_s) = \frac{9960}{T} - 2.75$

4.2.3 Experimental Measurement of Time to Carbon Boil

The measured time to the commencement of the carbon boil is measured from the experimental videos for comparison to the calculated results. The video recording setting recorded at a frequency of 30 Hz. Therefore an image once every approximately 0.033 seconds is available when performing frame by frame analysis.

In order to obtain consistent results an equal criterion must be applied to each measurement. In each experiment the droplet fell into the liquid slag. The precise instant where the carbon boil commences may not be directly observable since it occurs inside

the droplet. The criterion used to define the onset of the carbon boil in this study was the instant the downward momentum of the droplet was halted before rising. Drag and added mass forces can be expected to retard the downward motion of the droplet, but not cause it to rise[18]. Therefore, when the droplet begins to rise, it is taken as the result of internal evolution of gas. Visible expansion of the radius (droplet swelling) was observed soon after in each case, indicating that the cause for the droplet rising was internal gas evolution.

In the case of high FeO slags, the time to nucleation was seen to be very short. Given the high degree of motion of the droplet, a reliable determination of the time to internal nucleation was unable to be made. Therefore, measurements of this time were only taken in low FeO slags.

4.2.4 Model Results

The model was run up to the point of onset of internal nucleation as defined in Section 4.2.1. Model runs were made at varying FeO contents, C contents and S contents to see the variation in time to internal nucleation as an indicator of internal/external nucleation behaviour. Calculation runs where the criteria for internal nucleation is not met after long simulated reaction times indicate no expected carbon boil.

Results for a given set of calculation runs were put into a post processing program designed to calculate contours of time to internal nucleation time. Figure 4.6 gives results for a 0.005% S 1.0 g droplet. Individual data points represent experimental times to onset of the carbon boil as measured from experimental video analysis.

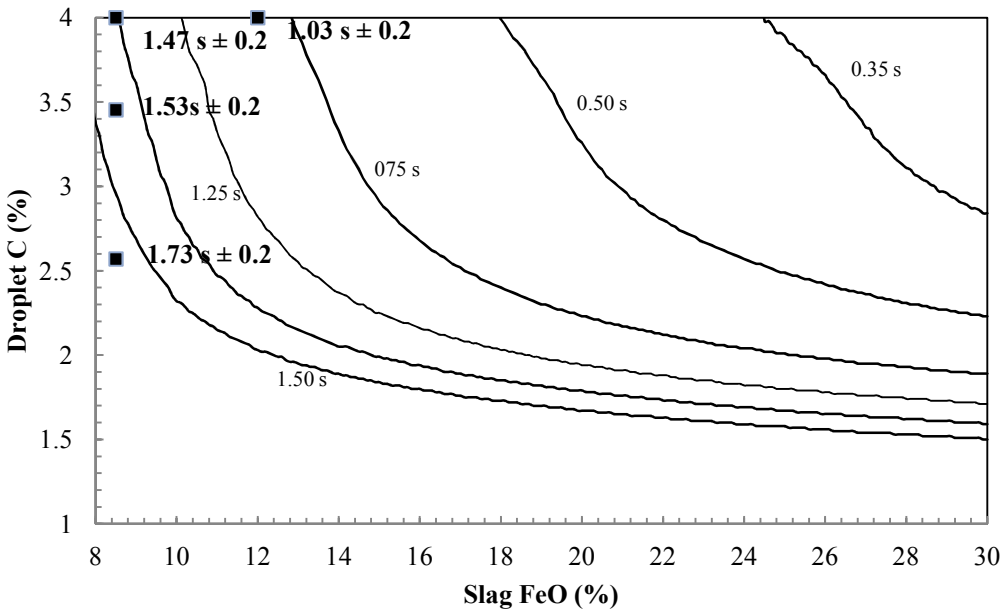

Figure 4.6 Calculated contours of time to onset of carbon boil.

It is seen that the onset of the carbon boil phenomenon is predicted to be highly dependent on both slag FeO content (O availability) and C content. The experimental points suggest that the onset of nucleation is later than predicted. This may be partially explained by the criterion used above to define experimental onset of nucleation, the arrest of downward motion of the droplet.

The effect of hot metal sulphur content can be seen schematically in Figure 4.7. By comparison to Figure 4.6 the output suggests that increasing sulphur content (at low S contents) facilitates the carbon boil. At 0 % S, it is seen that the model predicts the movement of the internal nucleation incubation time contours to higher FeO and C contents.

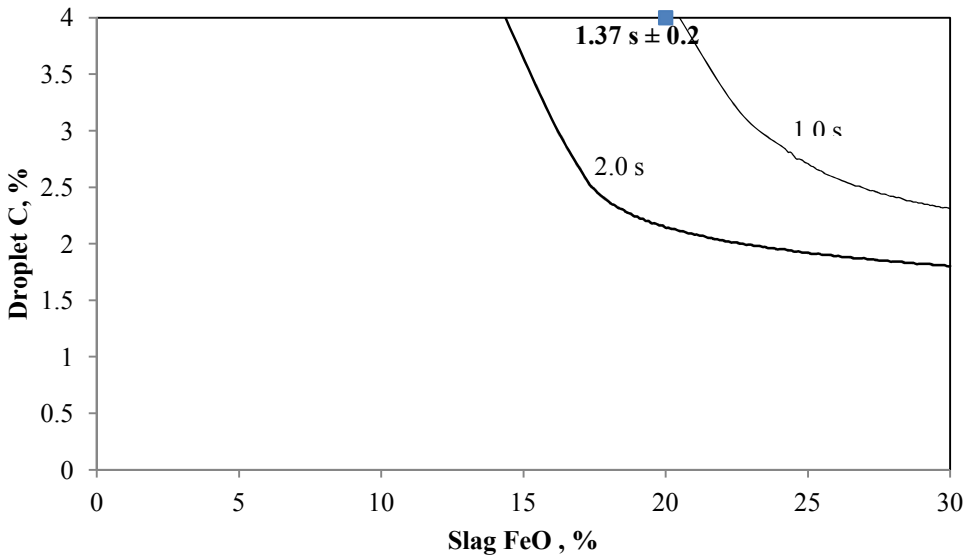

Figure 4.7 Calculated contours of time to onset of carbon boil at 0 % S content, 1 g. droplet.

At elevated sulphur levels, the computed effect of surface poisoning can be observed. Figure 4.8 shows the corresponding contour results for S = 0.030%.

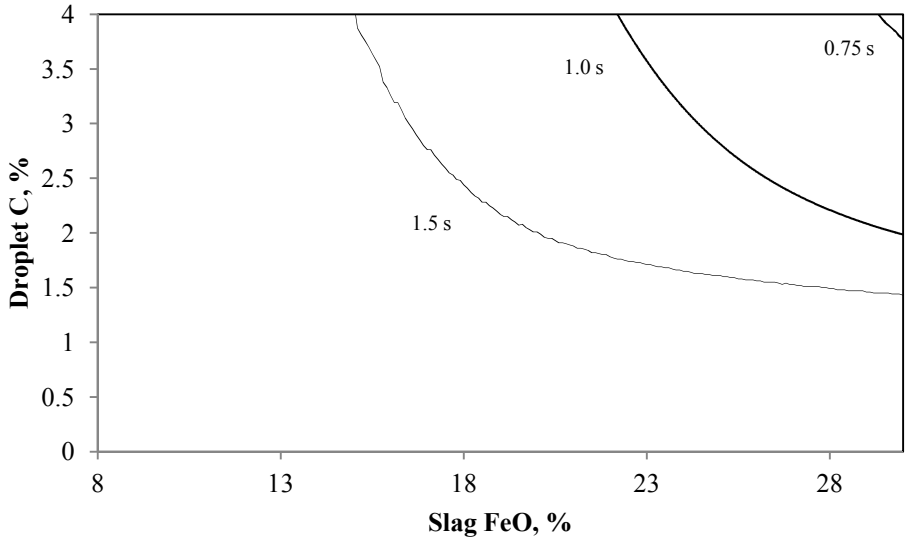

Figure 4.8 Calculated contours of time to onset of carbon boil at 0.030 % S content, 1 g. droplet.

Computational runs at different droplet masses were also carried out. A simulation at 2.0 g, 0.005% S is shown in Figure 4.9. It is seen, again by means of comparison to Figure 4.6, that the time to the commencement of carbon boil increases with increasing droplet mass.

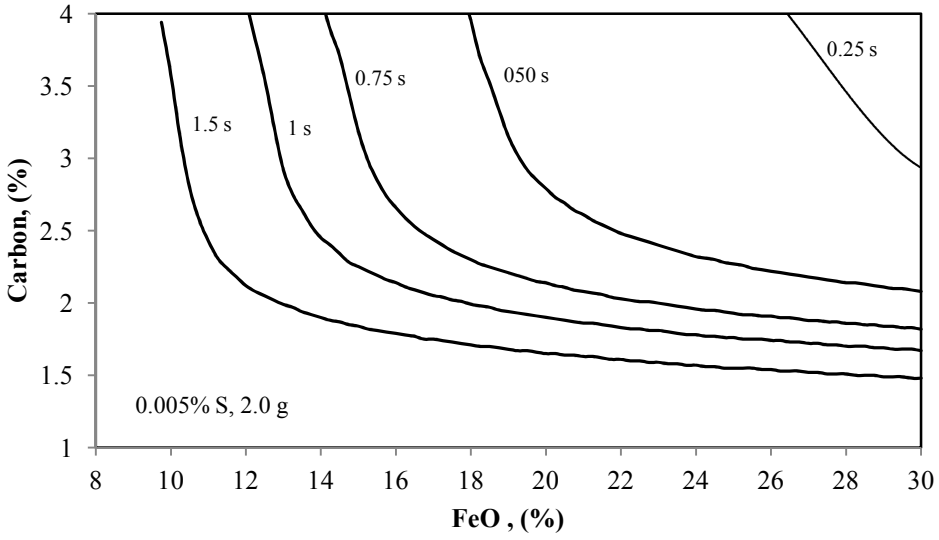

Figure 4.9 Calculated contours of time to onset of carbon boil at 2.0 g, 0.005%S.

4.3 Discussion

From Figure 4.2 it is apparent that slag FeO content, the availability of oxygen to the reaction system, plays an important role in driving reaction rate. This is to be expected as oxygen both provides driving force for the decarburization reaction itself and lowers the interfacial tension between gas and metal phases[30]. The trend seen in lower carbon droplets (2.5-2.9%) in Chen's work[19,20] is suggested to hold true by the results of the current experimental program at higher carbon (~4.25%).

Figure 4.10 gives a comparison of the present study's results to those in other studies.

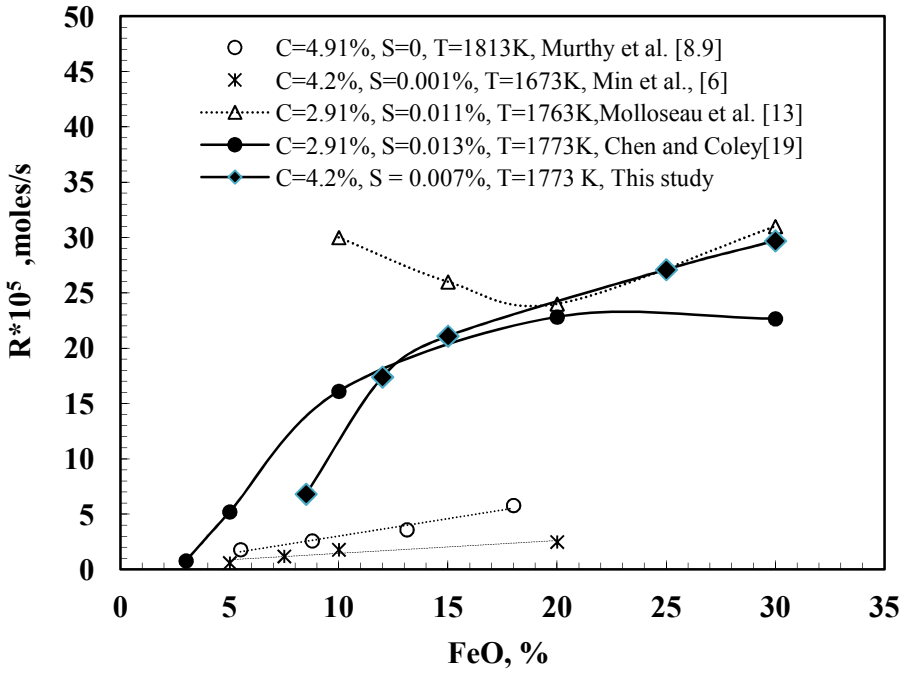

Figure 4.10: The present study's results in relation to other studies, adapted from Chen[19].

At high slag FeO contents (greater than approximately 12%), it is seen that the higher carbon droplets of the present study (4.25 %) exhibit a higher reaction rate than for the lower C droplets (~2.91%) in Chen's study[19]. Below 12% FeO, the lower C droplets have a faster evolution rate. The reason for this is not immediately clear although the S contents compared are slightly different (0.013 versus 0.007%). At low FeO contents, S content has a relatively greater influence on the interfacial tension as dissolved O decreases..

The dependence of decarburization rate on droplet mass is linear in both the case of the ~2.7 % C droplets of Chen[19] and ~4.2 % C droplets in the present study (Figure 4.11).

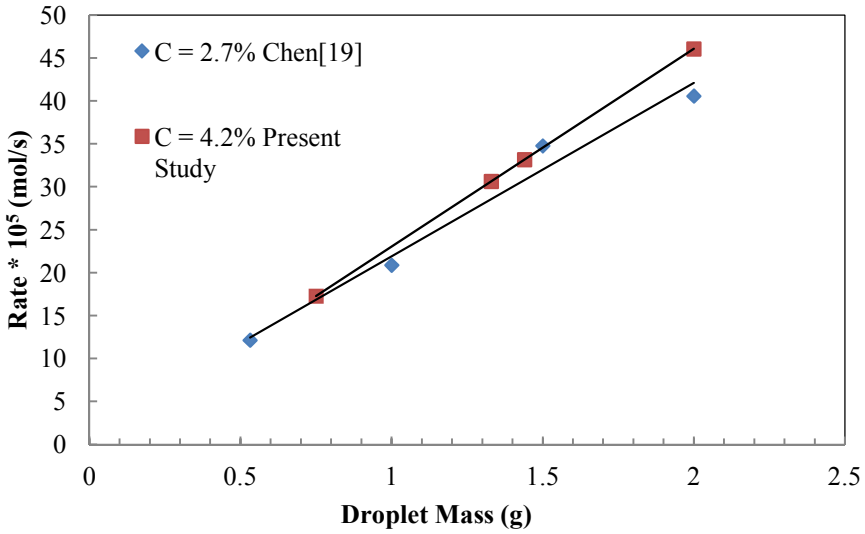

Figure 4.11 Comparison of droplet rate with mass at different initial C contents.

The difference in slope is expected due to the difference in driving force for the internal nucleation reaction.

Both the present study and Chen's[19] had similar variation with metallic sulphur content, exhibiting a maximum somewhere between 0.005 and 0.020 % S under similar experimental conditions. This behaviour is expected due to competing surface site blocking and surface tension depressing effects as per the analyses by Chen[19] and by Molloseau[13]: Sulphur is a surface active element in solution, lowering the surface tension. As the nucleation rate of bubbles is strongly dependent on surface tension (Rate

$\alpha \exp(-\sigma^3)$), it is expected that increasing S enhances the nucleation rate. Conversely since S is surface active it also blocks potential reaction sites.

The effect of the S in facilitating the carbon boil in low FeO slags can be analyzed by a model calculation run. S levels below the given lines in Figure 4.12 for specific carbon content are expected to give no internal evolution of gas for a given C content.

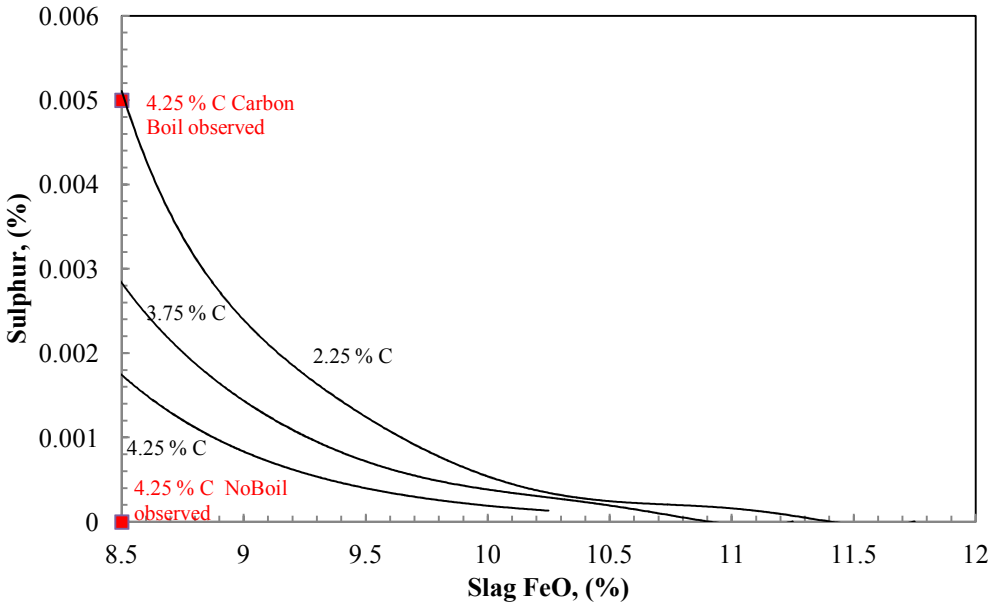

Figure 4.12: Calculated limit of carbon boil with varying S levels. Contours are constant in Carbon %.

The carbon boil phenomenon was observed over a wide range of experimental conditions. In particular, internal nucleation of gas was observed at slag FeO contents as low as 8.5% when S was approximately greater than 0.005%.

Min[6] observed no carbon boil in low FeO slags in the range 5-15 wt. % FeO at initial droplet carbon values similar to those used in the present study (~4.2%). The rate

was also seen to decay with increasing sulphur contents at all values for S. It is important to note the specific conditions under which Min's experiments were carried out. In general the droplet masses in Min's study were up to 5 times larger (5 g) than those achievable in the current study. The comparable cases between the two studies give reasonable agreement. Specifically, the lower mass droplet experiments in Min's study (1.5 – 2.0 g) are roughly comparable to the present study. In this case, S was nearly 0 in both cases (0 for the present study and 0.001 % for Min's). No carbon boil was observed in either case. Thus at low FeO content slags with low metal S levels, no internal evolution of gas is expected.

Min's experiments at higher slag FeO contents, up to 15%, were carried out with droplet masses much higher (4.2 – 5.1 g) than for the present work (0.5 – 2.0 g) and at low S contents (0.001%). Comparison of Figures 4.5 and 4.7 shows the effect of only a doubling of droplet mass. For 5.0 g droplets and very low S contents, no carbon boil is predicted numerically by the model.

Murthy's experiments[9,10] also showed no evidence of carbon boil at lower FeO contents (5-15%). However the S contents considered in Murthy's study were 0, 0.38% and 0.55% respectively. On the one hand 0 % S at low FeO contents (less than 12%) is expected to be unfavourable to internal CO evolution due to the higher surface tension. Conversely the high S contents of 0.38 and 0.55% selected in Murthy's study fall on the opposite end of the maxima with S content observed in the present work and in Chen's

study[19]. Therefore in these cases no discrepancy is believed to exist between the present work and Murthy's work.

4.4 Conclusions

1. Experiments carried out suggest that for higher carbon droplets (~4.2% C), CO evolution reaction rate is strongly dependent on slag FeO, S and droplet mass.

2. A numerical model encompassing diffusion driven transport of species in slag and metal, surface blockage of reaction sites and Chen's model for internal CO evolution[19,20] was able to predict the time to the onset of carbon boil and the presence of carbon boil with reasonable agreement with experimental results.

3. Sulphur plays a critical role in determining whether the carbon boil will take place or not, with droplets containing no sulphur at lower slag FeO contents exhibiting no internal gas evolution.

4. The rate of gas evolution goes through a maximum at approximately 0.007% S which appears to be due to the competing effects of sulphur on the rate of nucleation and the rate of oxygen pickup.

Appendix

A.1 Measurement of Initial Droplet C, S Contents

The accuracy of the LECO Carbon Sulphur Determinator used in the present study for measurement of carbon and sulphur contents was tested by running a series of standard samples to observe the consistency of measurements.

Figure A.1 shows the test results for a standard carbon samples with C = 3.664 % for 7 analysis runs.

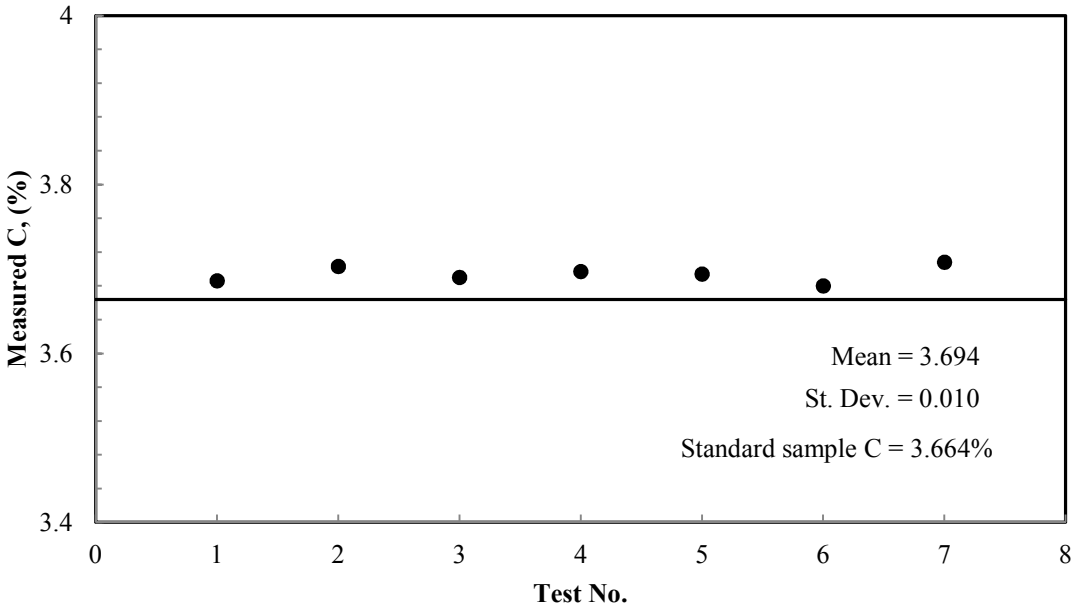

Figure A.1: 7 Test run results at standard of C = 3.664%.

The mean value obtained from the measurements is 0.030 % higher than the standard's stated composition. The standard deviation for the specimens is 0.010 for a mean measurement of 3.694.. This indicates a high degree of precision in carbon measurements used in this study.

Figure A.2 gives the results for sulphur for the corresponding test series shown in Figure A.1. The standard sample had a posted sulphur content of S = 0. 00616%.

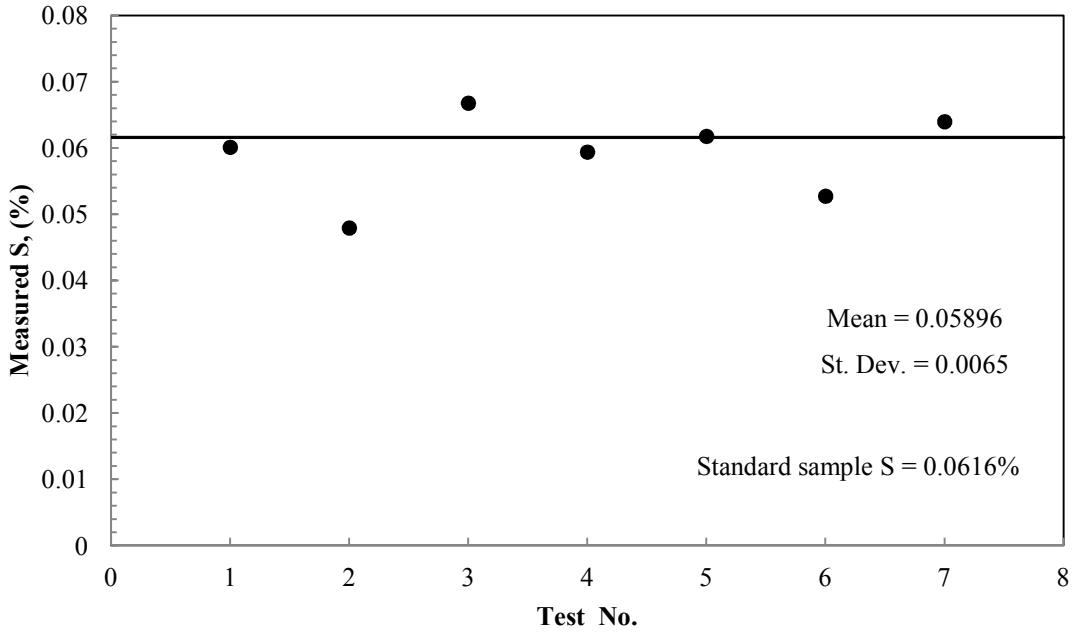

Figure A.2: Variation in measured S, for standard specimens with S = 0.0616%

It is seen that the deviation in S measurements is significantly larger for sulphur than for carbon. This is likely due to the smaller sulphur contents of the droplets to begin with, making deviations in the measurement more significant. As a result, stated sulphur contents have a lower degree of accuracy.

The method for preparation of the alloys used in the present study involved making successive additions of FeS to the Fe-C melt and allowing for homogenization before sampling. Therefore, assuming all FeS additions landed in the bath, it can be suggested at a bare minimum that successive samples contained increasing sulphur contents.

A.2 Oxygen During Preparation of Alloys

The high purity argon used during the preparation of alloys and the experiments has an oxygen content guaranteed less than 3 ppm. The maximum content of the Ar would therefore be 3 ppm. The presence of the sizeable graphite outer crucible puts the O_2 in the furnace working tube in equilibrium with solid graphite (C). This gives very small partial pressures of oxygen ($<10^{-14}$ atm) and the dissolved oxygen associated with these oxygen pressures is small (< 1 ppm). Indeed, it was observed during one case where the furnace seal broke during experimentation that a significant mass of the graphite crucible was reacted away under room atmospheres.

Oxygen could enter the alloy during transport from the furnace to the quenching bucket. Fick's second law is applied to calculate the diffusion distance for oxygen into liquid iron (surface oxygen in equilibrium with air as the highest limiting case) and for γ iron. The diffusion distance from the surface was (rounded up to nearest millimeter) 5 mm and 2 mm respectively. Therefore specimens for experiments were taken only from at least 2 cm from the air exposed surface.

References

1. J.M. Gaines. *BOF Steelmaking: Introduction, Theory and Design Part I.* 1982: The Iron and Steel Society, pp. 1-22.

2. H.W. Meyer, W.F. Porter, G.C. Smith & J. Szekely: *Journal of Metals,* 1968, pp. 35-42.

3. G.H. Geiger, P. Kozakevitch, M. Olette & P.V. Riboud. *BOF Steelmaking: Introduction, Theory and Design Part I.* 1982: The Iron and Steel Society, pp. 302-431.

4. P. Kozakevitch: *Journal of Metals,* 1969 (July), pp.57-68.

5. E.W. Mulholland, G.S. Hazeldean & M. Davies: *J. Iron Steel Inst.* , 1973 (September), pp. 632-639.

6. D.J. Min & R.J Fruehan: *Met. Trans. B,* 1992, vol. 23B, pp.29-37.

7. R.H. Smith & R.J. Fruehan: *Steel Research,* 1999, vol. 70, no 8+9, pp. 283-295

8. G.G. Krishna Murthy, Y. Sawada & J.F. Elliot: *Iron. & Steelmaking,* 1993, vol. 20, no.3, pp. 179-190

9. G.G. Krishna Murthy, A. Hasham & U.B. Pal: *Iron. & Steelmaking,* 1993, vol. 20, no.3, pp. 191-200

10. F.J Mannion & R.J. Fruehan: *Met. Trans. B,* 1989, vol. 20B, pp. 853-861.

11. T. Gare & G.S.F. Hazeldean: *Iron. & Steelmaking,* 1981, no.4, pp. 169-181.

12. H. Gaye & R.V. Riboud: *Met. Trans. B,* 1977, vol. 8B, pp. 409-415.

13. C.L. Molloseau & R.J. Fruehan: *Met. Trans. B,* 2002, vol. 33B, pp. 335-344.

14. H. Sun: *ISIJ Int.,* 2006, vol. 46, no. 11, pp. 1560-1569.

15. L.A. Baker & R.J. Ward: *J. Iron Steel Inst.,* 1967 (July), pp. 714-717.

16. L.A. Baker, N.A. Warner & A.E. Jenkins: *Trans. Met. Soc. AIME,* 1967, vol. 239, pp.857-864.

17. Subagyo, G.A. Brooks & K.S. Coley: *Can. Met. Quart.,* 2005, vol. 44, no.1 pp. 119-130.

18. G. Brooks, Subagyo, Y. Pan & K. Coley. *Met. Mat. Trans. B.,* Vol. 36B, (August), pp. 525-535.

19. E. Chen & K.S. Coley*, Ironmaking & Steelmaking*, 2010, Vol. 37, pp. 541-545.

20. E. Chen , McMaster University, Personal Correspondence: Ph.D. Thesis Draft.

21. D.J. Price, *Process Engineering of Pyrometallurgy*, 1974, pp. 8-15.

22. H-Y. Kwak, S-D. Oh: *J. Coll. Interfac. Sci.,* 1998*,* vol. 198, pp. 113-118.

23. S.D. Lubetkin: *Langmuir*, 2003*,* vol. 19, pp. 2575-2587.

24. R.C. Tolman: *J. Chem. Phys.,* 1949, vol. 17, no.3, pp. 333-337.

25. H.S. Levine: *Met. Trans.,* 1973, vol. 4, pp. 777-782.

26. H S. Levine: *J. Phys.Chem.*, 1972, Vol.76, No.18, pp.2609-2614

27. D.G.C. Robertson & A.E. Jenkins: *Heterogeneous Kinetics at Elevated Temperatures,* 1970, pp. 393-408.

28. P.G. Bowers, K. Bar-Eli, R.M. Noyes: *J. Chem. Soc., Faraday Trans.,* 1996, vol. 92, no. 16, pp. 2843-2849.

29. G.R. Belton: *Met. Trans. B.,* 1976, Vol. 7B, pp. 35 – 42.

30.J. Jimbo, a. Sharan and A. Cramb: *Steelmaking Conference Proceedings (ISS).,* 1993, pp.485 – 494.

31. D.R.Sain and G.R.Belton, *Met.and Matls. Trans. B, 1976, Vol.* 7B,(1976): 235

32. S. Basu, A. Lahiri, S. Seetharaman: *Met. Matls. Trans. B.,* 2008, Vol. 39B, pp. 447 – 456.

33. F. Hesterkamp, K. Lohberg: Arch. fur das Eis., vol. 37, 1966, pp. 813 – 819.

34. M. Kawakami, S. Yokoyama, K. Takagi, M. Nishimura & J. Kim: *ISIJ Int.*, Vol. 37, 1997, 425.

35. Steelmaking Data Sourcebook, The Japan Society for Promotion of Science, The 19th Committee onSteelmaking,1998.

36. E. Sibata, H. Sun, K. Mori: Met. Matls. Trans. B., 1999, Vol. 30B, pp. 279-286.

37. V. Carey, Liquid-Vapor Phase Change Phenomena. 2008, New York, Taylor and Francis.